

Title: STING induces HOIP-mediated synthesis of M1 ubiquitin chains to stimulate NF κ B signaling

Authors: Tara D. Fischer^{1*}, Eric N. Bunker¹, Peng-Peng Zhu¹, François Le Guerroué^{1†‡}, Mahan Hadjian¹, Eunice Dominguez-Martin¹, Francesco Scavone^{2§}, Robert Cohen², Tingting Yao², Yan Wang³, Achim Werner⁴, and Richard J. Youle^{1*}

Affiliations:

¹ Biochemistry Section, Surgical Neurology Branch, National Institute of Neurological Disorders and Stroke, National Institutes of Health; Bethesda, MD, USA.

² Department of Biochemistry and Molecular Biology, Colorado State University; Fort Collins, CO, USA.

³ Mass Spectrometry, National Institute of Dental and Craniofacial Research, National Institutes of Health; Bethesda, MD, USA.

⁴ Stem Cell Biochemistry Unit, National Institute of Dental and Craniofacial Research, National Institutes of Health; Bethesda, MD, USA.

* Corresponding author. Emails: fischertad@nih.gov and youler@ninds.nih.gov

Present Address:

† Université Paris-Saclay, Commissariat à l'Energie Atomique et aux Energies Alternatives, CNRS, Laboratoire des Maladies Neurodégénératives: Mécanismes, Thérapies, Imagerie; 92265 Fontenay-aux-Roses, France.

‡ Université Paris-Saclay, Commissariat à l'Energie Atomique et aux Energies Alternatives, Molecular Imaging Research Center; 92265 Fontenay-aux-Roses, France.

§ Department of Biology, Stanford University; Stanford, CA, USA.

Abstract

STING activation by cyclic dinucleotides in mammals induces IRF3- and NF κ B -mediated gene expression, and the lipidation of LC3B at Golgi-related membranes. While mechanisms of the IRF3 response are well understood, the mechanisms of NF κ B activation mediated by STING remain unclear. We report that STING activation induces linear/M1-linked ubiquitin chain (M1-Ub) formation and recruitment of the LUBAC E3 ligase, HOIP, to LC3B-associated Golgi membranes where ubiquitin is also localized. Loss of HOIP prevents formation of M1-Ub ubiquitin chains and reduces STING-induced NF κ B and IRF3-mediated signaling in human monocytic THP1 cells and mouse bone marrow derived macrophages, without affecting STING activation. STING-induced LC3B lipidation is not required for M1-Ub chain formation or the immune-related gene expression, however the recently reported function of STING to neutralize the pH of the Golgi may be involved. Thus, LUBAC synthesis of M1 ubiquitin chains mediates STING-induced innate immune signaling.

Keywords: Golgi/Innate Immunity/Interferon/LUBAC/LC3B

Introduction

The evolutionarily conserved cGAS-STING pathway initiates potent innate immune responses through several signaling cascades following the detection of double-stranded DNA (dsDNA) in the cytoplasm of cells (Chen *et al*, 2016; Hopfner & Hornung, 2020; Ahn & Barber, 2019). In mammals, cGAS synthesizes the cyclic dinucleotide 2'3' cyclic GMP-AMP (cGAMP) and its binding to STING at ER membranes induces the trafficking of STING from the ER to the Golgi apparatus. Following trafficking through Golgi compartments, and prior to its degradation in the lysosome, STING initiates a broad transcriptional program of type I interferons mediated by its interaction with the kinase TBK1 and the transcription factor IRF3. At Golgi membranes, active STING also induces the lipidation of the ubiquitin-like protein, LC3B, through mechanisms that are distinct from the known role of LC3B lipidation in autophagosome formation (Gui *et al*, 2019; Fischer *et al*, 2020; Mizushima, 2020). Activation of cGAS-STING also induces the transcription of NF κ B related genes through poorly understood mechanisms (Ishikawa & Barber, 2008; Abe & Barber, 2014; Mann *et al*, 2019; Balka *et al*, 2020; Yum *et al*, 2021). Although all of these downstream signaling events mediated by STING activation have been reported to play a role in antiviral defense (Gui *et al*, 2019; Ishikawa & Barber, 2008; Yum *et al*, 2021; Zhong *et al*, 2008;

Ishikawa *et al*, 2009), whether and how they are mechanistically related is unclear. Here, we report that ubiquitin robustly co-localizes with activated STING and LC3B at Golgi membranes. As ubiquitylation is important in both autophagy-related and innate immune signaling, we sought to determine whether these ubiquitylation events play a role in STING-mediated innate immune responses.

STING activation induces M1- and K63- ubiquitin chain formation.

Activation of STING and its trafficking to the perinuclear region of cells induces clusters of small LC3B positive vesicles near the Golgi apparatus (hereafter referred to as LC3B foci) (Gui *et al*, 2019; Fischer *et al*, 2020; Prabakaran *et al*, 2018). Immunostaining for ubiquitin (Ub) after treatment with the STING ligand, 2'3 cGAMP, or the STING agonist diABZI, in HeLa cells stably expressing untagged STING (HeLa^{STING}), at low levels, and mEGFP-LC3B showed that >80% of cells present Ub positive foci that co-localize with mEGFP-LC3B and a subset of STING punctae in the perinuclear region (**Fig. 1A,B and EV1**).

Ubiquitin can be conjugated to other ubiquitin molecules at any of the seven lysine residues and to the N-terminal methionine (M1), forming unique polyubiquitin chains that mediate specific downstream signaling pathways (Komander & Rape, 2012). To detect which polyubiquitin chain species are localized at LC3B-foci, we used linkage specific ubiquitin antibodies to immunostain for K48- and K63-Ub chains (**Fig. EV1**). Robust K63-Ub positive foci were detected in 67% of cells, with over 80% of mEGFP-LC3B foci staining positively for K63-Ub (**Fig. EV1**). However, no K48-Ub foci were detected in cells, and no mEGFP-LC3B foci stained positively for K48-Ub (**Fig. EV1**). K63-Ub co-localization with LC3B following STING activation by cGAMP or diABZI in live cells was also detected using a fluorescently tagged probe that selectively binds K63-Ub chains (Sims *et al*, 2012) (**Fig. EV1 and Movie 1**). Consistently, detection of linkage-specific polyubiquitin chains by immunoblotting showed a cGAMP-induced increase in K63-Ub, but not K48-linked or total-Ub (**Fig. 1C-E, G**). By immunoblotting, we also probed for linear/M1-linked ubiquitin chains (hereafter referred to as M1-Ub) following STING activation. Surprisingly, cGAMP activation of STING induced a robust increase in M1-Ub chains (**Fig. 1F,G**). To confirm the distinct polyubiquitin chains independently of antibody detection, we used mass spectrometry to quantitatively identify GG-K/M linked peptides in cells following STING activation (**Fig. 1H**). Detection of GG-K/M linked peptide abundances in lysates from untreated and cGAMP treated cells showed a small increase in GG-K(63) peptides, and no change in GG-K(48) peptides (**Fig. 1H**). M1-Ub chains

were detected after enrichment for ubiquitin using Pan-TUBE (Tandem Ubiquitin Binding Entities) pulldown, showing an eight-fold average increase in GG-M(1) peptide abundance with cGAMP treatment compared to the untreated control (**Fig. 1H**). Collectively, these data demonstrate that STING activation induces robust ubiquitin co-localization with LC3B foci in the perinuclear region, that prior work showed is the Golgi apparatus (Fischer *et al*, 2020; Gui *et al*, 2019; Liu *et al*, 2023; Xun *et al*, 2023). STING activation also induces the synthesis of M1 ubiquitin chains, in addition to K63 ubiquitin chains.

LC3B lipidation at acidic organelles can be induced by a variety of stimuli, including lysosomotropic agents, such as Monensin (also referred to as CASM) (Jacquin *et al*, 2017). To determine whether ubiquitin co-localization with LC3B is a general feature of LC3B lipidation at acidic organelles, we immunostained for ubiquitin following Monensin treatment (**Fig. 1I**). Ubiquitin was detected at some, but not all, Monensin-induced LC3B vesicles (**Fig. 1I**). Immunoblotting for K63- and M1-Ub chains following Monensin treatment showed an increase in K63-Ub chains, but not M1-Ub chains (**Fig. 1J-L**), indicating that M1-Ub chain formation may be selectively associated with STING-mediated LC3B lipidation at Golgi membranes.

HOIP is required for STING activation-induced M1-Ub chain formation in HeLa and immune cell lines.

While many E3 ligases generate K63 ubiquitin chains, M1 ubiquitin chains are only known to be formed by the E3 ligase HOIP, a component of the Linear Ubiquitin Assembly Complex (LUBAC) (Kirisako *et al*, 2006; Sasaki & Iwai, 2015). Stable overexpression of mEGFP tagged HOIP in HeLa^{STING} cells also stably expressing mScarletI-LC3B, showed a cytosolic localization in untreated cells (**Fig. EV2**). cGAMP activation of STING induced a clustering of mEGFP-HOIP in the perinuclear region that co-localized with mScarletI-LC3B foci and STING (**Fig. 2A,B, EV2**). The localization of mEGFP-HOIP was further resolved following a brief saponin extraction prior to fixation (**Fig. 2A, EV2**), indicating a stable association with LC3B labeled perinuclear Golgi structures. The colocalization of HOIP and LC3B foci suggests that the ubiquitin species detected there may be M1-Ub chains, in addition to K63-Ub.

To determine whether HOIP is required for M1-Ub chain formation induced by STING activation, we generated a HOIP knockout HeLa cell line (HOIPKO HeLa^{STING}). M1-Ub chains following STING activation by either cGAMP (**Fig. 2C,E, and EV2**) or diABZI (**Fig. EV2**) were eliminated in HOIPKO HeLa^{STING} cells, while K63-Ub chains were unaffected (**Fig. EV2**). Stable reconstitution of HOIP in HOIPKO HeLa^{STING} cells rescued

M1-Ub chain formation following cGAMP activation of STING, confirming that HOIP is required for STING induced M1-Ub chain formation (**Fig. 2C,D**). Stable overexpression of the M1 ubiquitin-specific deubiquitylase OTULIN in HeLa^{STING} cells, which has been shown to counteract HOIP's E3 ligase activity (Fiil *et al*, 2013; Keusekotten *et al*, 2013), also eliminated M1-Ub chains, but not K63-Ub chains, following STING activation (**Fig. EV2**).

STING activation, indicated by LC3B lipidation and phosphorylation of STING at serine 366 following either cGAMP or diABZI treatment was largely unaffected in HOIPKO HeLa^{STING} cells over time (**Fig. EV2**). OTULIN overexpression also causes no difference in LC3B lipidation or STING phosphorylation following cGAMP treatment (**Fig. EV2**). While there appeared to be a modest disruption of STING degradation at later timepoints in HOIPKO HeLa^{STING} cells following either cGAMP or diABZI treatment (**Fig. EV2**), this effect was not rescued with HOIP reconstitution (**Fig. 2C**), and not observed with endogenous STING in HOIPKO HeLa cells (**Fig. EV2**), or in OTULIN overexpressing HeLa^{STING} cells (**Fig. EV2**). We further sought to determine whether STING induces HOIP synthesis of M1-Ub chains and the effect of HOIP loss on STING signaling in well-established, immune-relevant cell models with robust endogenous STING expression. Activation of endogenous STING with either cGAMP or diABZI in the human monocyte, THP1, cell line (**Fig. 2E-G and EV2**), and diABZI in an immortalized mouse bone marrow derived macrophage cell line (**Fig. 2H,I**), induced formation of M1-Ub chains. Loss of HOIP in THP1 cells (HOIPKO^{pool}) (**Fig. 2E-G, and EV2**) or knock down of HOIP in iBMDMs by shRNA (shHOIP) (**Fig. 2H,I**) substantially reduced the detection of M1-Ub chains following STING activation. M1-Ub chain formation following STING activation was rescued by stable reconstitution of HOIP in HOIPKO^{pool} THP1 cells (**Fig. 2E-F**). Further, LC3B lipidation and STING degradation were unaffected in HOIPKO^{pool} THP1 cells (**Fig. 2E-G, and EV2**), and shHOIP iBMDMs (**Fig. 2H,I**) following cGAMP or diABZI activation of STING. These results demonstrate that STING activation induces HOIP synthesis of M1-Ub chains in multiple cell lines, and loss of HOIP does not affect STING activation or key downstream events in the STING pathway.

Loss of STING-mediated VAIL disrupts the perinuclear localization of ubiquitin and HOIP, but not M1-Ub chain formation.

While examining the spatial localization of ubiquitin following STING activation, we found that stable overexpression of mEGFP-LC3B in HeLa^{STING} cells more tightly condenses both ubiquitin and STING into perinuclear foci (**Fig. EV3**) and increases the detection of M1-Ub ubiquitin chains by immunoblotting following cGAMP treatment (**Fig. EV3**). As HOIP is not required for STING induced LC3B lipidation (**Fig. 2 and EV2**), we questioned whether LC3B lipidation may function upstream of M1-Ub chain formation following STING activation. We previously reported that STING activation induced LC3B lipidation is distinct from autophagosome formation and occurs through a process we termed V-ATPase-ATG16L1 induced LC3B lipidation (VAIL) at single membrane, Golgi-related vesicles (Fischer *et al*, 2020). The bacterial effector, SopF, blocks recruitment of ATG16L1 to the V-ATPase and STING-mediated LC3B lipidation, without affecting autophagy, presenting a useful tool to selectively disrupt VAIL (Xu *et al*, 2019; Fischer *et al*, 2020; Xu *et al*, 2022). Comparison of HeLa^{STING} cells with or without stable expression of SopF showed no substantial difference in M1-Ub chain formation detected by immunoblotting (**Fig. 3A**), however ubiquitin foci formation was blocked following cGAMP treatment (**Fig. 3B**). Similarly, elimination of LC3B lipidation by loss of ATG16L1 caused no effect on STING-mediated M1-Ub chain formation (**Fig. 3C**), whereas ubiquitin and mEGFP-HOIP foci formation were blocked (**Fig. 3F,G**) in ATG16L1KO HeLa^{STING} cells. Further examination of ubiquitin and mEGFP-HOIP localization with saponin extraction in WT and ATG16L1KO HeLa^{STING} cells following diABZI activation of STING showed that ubiquitin and mEGFP-HOIP appear in small, dispersed punctae, rather than larger, clustered foci (**Fig. 3F-G**). It has recently been reported that STING may form a proton channel in Golgi membranes upon its activation and trafficking that neutralizes the pH of the Golgi and stimulates LC3B lipidation (Liu *et al*, 2023; Xun *et al*, 2023). C53 is a small molecule agonist of STING that is reported to block LC3B lipidation and the neutralization of Golgi pH following STING activation by binding to the putative proton channel region in STING's transmembrane domains (Liu *et al*, 2023; Xun *et al*, 2023; Pryde *et al*, 2021). Treatment of HeLa^{STING} cells with C53 blocked STING activation induced LC3B lipidation, and partially reduced M1-Ub chain formation (**Fig. EV3**) following diABZI treatment. Live imaging of mScarlet1-LC3B and the K63-Ub sensor, Vx3-mEGFP, also demonstrated that C53 blocks both LC3B and Vx3 foci formation in the perinuclear region (**Fig. EV3**). Collectively, these results indicate that the lipidation of LC3B is not required for STING-

induced HOIP synthesis of M1-Ub chains but affects the spatial localization of ubiquitin and HOIP. The Golgi pH neutralizing activity of STING may also be involved upstream of both M1-Ub chain formation, ubiquitin localization, and LC3B lipidation, indicating a possible shared signal that induces these processes at the same membranes.

M1 ubiquitin chains stimulate STING-mediated NF κ B signaling.

Whereas K63 ubiquitin chains have been associated with diverse cellular functions, M1 ubiquitin chains are most widely understood to function in immune signaling, particularly through the NF κ B pathway (Tokunaga *et al*, 2009; Rahighi *et al*, 2009; Haas *et al*, 2009; Sasaki & Iwai, 2015). Since activation of STING induces NF κ B signaling in addition to IRF3 mediated signaling, we asked whether M1 ubiquitin chain formation induced by STING activation mediates NF κ B signaling. HeLa cells overexpressing STING displayed differences in IRF3- and NF κ B-related gene expression between HOIPKO and OTULIN overexpressing cell lines (**Appendix Fig. S1**). To avoid potential clonal variation in our HOIPKO line, complications from STING overexpression, and to study a more immune-relevant cell model, we assessed immune signaling in our HOIPKO^{pool} THP1 monocyte cells. In WT and HOIPKO^{pool} THP1 cells, we assessed markers for both IRF3- and NF κ B-related signaling by immunoblotting and gene expression following STING activation by either cGAMP (**Fig. EV4**) or diABZI (**Fig. 4**). In WT THP1 cells, robust phosphorylation of IRF3 at serine 386 and TBK1 at serine 172 were detected at the one-hour timepoint post diABZI treatment (**Fig. 4A**), and the two-hour timepoint post cGAMP treatment (**Fig. EV4**). No differences in these events were observed in HOIPKO^{pool} THP1 cells with either treatment (**Fig. 4A and Fig. EV4**). Detection of the degradation of the NF κ B inhibitor, I κ B α , at the 4-hour time point post diABZI (**Fig. 4A**) or cGAMP (**Fig. EV4**) treatment in WT cells showed no substantial defect in the HOIPKO^{pool} THP1 cells. However, the phosphorylation of I κ B α at serine 32 appeared to be delayed in the HOIPKO^{pool} THP1 cells compared to WT with both treatments (**Fig. 4A,B and EV4**). Reconstitution of HOIP in HOIPKO^{pool} THP1 cells, rescued the phosphorylation of I κ B α following diABZI activation of STING (**Fig. 4C,D**).

Consistent with reduced upstream activation of the NF κ B pathway, transcription of the NF κ B-related genes, *TNF*, *TNFAIP3*, and *IL6* were reduced in HOIPKO^{pool} THP1 cells following both diABZI (**Fig. 4C**) and cGAMP treatments (**Fig. EV4**). Despite no changes in IRF3 phosphorylation (**Fig. 4A**), STING activation

induced expression of the IRF3-mediated gene, *IFN β* , by both diABZI (**Fig. 4D**) and cGAMP (**Fig. EV4**) was reduced in HOIPKO^{pool} THP1 cells. However, interferon β -mediated gene expression was unaffected by loss of HOIP (**Fig. 4D and EV4**). These results may reflect cross regulation of *IFN β* gene induction by NF κ B, in line with previous reports (Abe & Barber, 2014). Reconstitution of HOIP in HOIPKO^{pool} THP1 cells, rescued NF κ B and IRF3 related gene expression following diABZI treatment (**Fig. 4C,D**). Consistent with results in THP1 cells, reduced expression of NF κ B- and IRF3- genes was also observed with the knock down of HOIP in iBMDMs following diABZI activation of STING (**Fig. EV4**). These data indicate that HOIP is important for STING activation induced NF κ B and IRF3-related signaling in human THP1 monocytes, and mouse bone marrow derived macrophages.

LC3B lipidation is not required for STING-mediated innate immune responses.

Since our discovery that STING activation induced LC3B lipidation is distinct from autophagy (Fischer *et al*, 2020), it has been unclear what the function of this process is in STING-mediated innate immunity. Although loss of LC3B lipidation induced by STING activation did not affect M1-Ub chain formation (**Fig. 3**), we questioned whether the potential regulation of ubiquitin and HOIP spatial localization we observed (**Fig. 3**) may impact downstream IRF3- and NF κ B-related signaling. To address this question, we examined STING activation in ATG16L1KO THP1 cells. Compared to WT controls, M1-Ub chain formation induced by diABZI treatment was unaffected in ATG16L1KO THP1 cells (**Fig. 5A**), similarly to HeLa cells (**Fig. 3C,D**). While a defect in STING degradation was detected (**Fig. 5A**), similarly to previous reports (Gentili *et al*, 2023), phosphorylation of IRF3, TBK1, and I κ B α were unchanged by the loss of ATG16L1 (**Fig. EV5**). Consistently, no differences between WT and ATG16L1KO THP1 cells were observed in IRF3/interferon- or NF κ B-related gene expression following STING activation by diABZI (**Fig. 5B,C**), despite small, but significant increases in ATG16L1KO cells at the 8 hour time point in *TNF* and *TNFAIP3* induction (**Fig. 5B**). We also examined the effect of C53-mediated inhibition of LC3B lipidation on immune-related signaling. Although no substantial differences were observed in diABZI-induced phosphorylation of I κ B α with C53 treatment (**Fig. EV5**), C53 treatment reduced NF κ B and IRF3-related gene expression (**Fig. EV5**). These results indicate that LC3B lipidation induced by STING activation does not regulate M1-Ub chain formation or IRF3- and NF κ B-related

gene expression. However, the upstream consequences of the reported proton channel activity of STING may regulate both, as well as LC3B lipidation, at Golgi membranes.

Discussion

Innate immune responses to cytosolic DNA, from viruses, bacteria, mitochondria or the nucleus are mediated in part by cGAS activation of STING (Ablasser & Chen, 2019). Following the detection of dsDNA, mammalian cGAS synthesizes the cyclic dinucleotide, 2'3' cGAMP, that binds to STING and induces its membrane trafficking from the ER to the Golgi apparatus. STING localization at the Golgi and Golgi-related vesicles, initiates IRF3- and interferon-related immune signaling and LC3B lipidation at Golgi membranes, prior to its degradation in the lysosome. STING activation also induces NF κ B transcriptional responses, which confers an important interferon-independent antiviral signature of STING signaling (Ishikawa & Barber, 2008; Abe & Barber, 2014; Mann *et al*, 2019; Balka *et al*, 2020; Yum *et al*, 2021). However, the mechanism of NF κ B activation by STING, and the relation to other signaling cascades induced by STING activation and trafficking have remained unclear. We find that STING activation induces the localization of the Linear Ubiquitin Chain Assembly Complex (LUBAC) E3 ligase, HOIP, at LC3B-associated Golgi membranes and its synthesis of M1-linked/linear ubiquitin (M1-Ub) chains to stimulate NF κ B-related immune signaling. Loss of HOIP prevents M1-Ub chain formation following STING activation by multiple agonists, which impairs I κ B α phosphorylation, and the expression of NF κ B-related genes. IRF3-related gene expression is also reduced with the loss of HOIP, even though STING, IRF3, and TBK1 phosphorylation remain intact, aligning with potential cross regulation between IRF3 and NF κ B-related gene expression (Abe & Barber, 2014). While our work has revealed a key mechanistic step in NF κ B signaling mediated by STING, several questions remain regarding how M1-Ub chains regulate NF κ B signaling. The markedly slower kinetics and persistence of M1-Ub chain formation and p-I κ B α we report with both cGAMP and diABZI stimulation of STING suggests distinct mechanisms compared to the quickly activated and resolved responses following TNFR or IL1R stimulation (Haas *et al*, 2009; Emmerich *et al*, 2013; Tarantino *et al*, 2014; Ruland, 2011). The recruitment of HOIP to the perinuclear region of cells also raises intriguing questions related to the spatial regulation of LUBAC activity and substrate specificity. Although we were unable to determine whether M1-Ub chains, specifically, are localized in

perinuclear foci with LC3B, the localization of HOIP is highly suggestive that M1-Ub may be a ubiquitin species detected at these sites. Overcoming the limitations of linkage-specific ubiquitin cross reactivity (Matsumoto *et al*, 2012) and more reliable reporters will be necessary to further study the spatial localization of M1-Ub chains following STING activation and in other pathways. K63-Ub are one ubiquitin species detectably localized with LC3B foci in the perinuclear region upon STING activation. It will be interesting to determine if these K63 ubiquitin chains are homotypic or heterotypic with M1 ubiquitin chains (i.e., hybrid K63/M1-Ub chains) (Emmerich *et al*, 2013) or conjugated to specific substrates, and whether the K63-Ub chains play distinct or related roles with M1-Ub chains in STING-induced innate immune signaling. Indeed, STING itself is reported to be conjugated to K63 ubiquitin chains (Tsuchida *et al*, 2010; Zhang *et al*, 2012; Ni *et al*, 2017; Kuchitsu *et al*, 2023; Prabakaran *et al*, 2018; Takahashi *et al*, 2021), which is important for its degradation (Kuchitsu *et al*, 2023). Unravelling the specific characteristics of these ubiquitin chains will be necessary to understand how they regulate the cGAS-STING pathway.

While our study began by investigating the ubiquitin species localized with LC3B in perinuclear foci we found that STING activation stimulates M1-Ub chain formation and LC3B lipidation in parallel. LC3B lipidation induced by STING is not required for formation of M1-Ub chains, and HOIP synthesis of M1-Ub chains is not required for LC3B lipidation, in multiple cell lines. However, we observed that loss of LC3B lipidation affects the spatial localization of HOIP and ubiquitin in perinuclear foci in HeLa cells, suggesting that LC3B lipidation may be involved in remodeling of their resident membranes. Importantly, while LC3B lipidation has been a recognized consequence of STING activation, the function of this process independently of autophagy, has not been resolved. Here, we show that LC3B lipidation is not required for STING-mediated IRF3- or NF κ B-related immune signaling. These results suggest that the effect of LC3B lipidation on the spatial localization of ubiquitin and HOIP may be dispensable for immune-related transcriptional regulation following STING activation. Indeed, transcription factor activation independent of spatial location would be consistent with previous reports on STING signaling and other pattern recognition receptor pathways (Dobbs *et al*, 2015; Tan & Kagan, 2019; Landau *et al*, 2024). Further, we show that inhibition of the recently reported channel activity of STING by the small molecule, C53, that inhibits LC3B lipidation, also partially inhibits STING-mediated M1-Ub and K63-Ub localization, as well as NF κ B- and IRF3-related gene expression. These results suggest that the potential proton channel activity of STING and its neutralization of the Golgi pH may be a shared upstream

signal stimulating these responses at Golgi membranes. Much more work is necessary to unravel the signaling and membrane dynamics between STING, ubiquitin, and LC3B, at the Golgi and how the combination of these processes shape STING-mediated innate immunity.

Materials and Methods

Reagents and Tools Table

Reagent/Resource	Reference or Source	Identifier or Catalog Number
Experimental Models		
HeLa	ATCC	CVCL_0300
HEK293T	ATCC	#CRL-3216
HOIPKO HeLa	This paper	
ATG16L1KO HeLa	Fischer et al., 2020	
WT THP1 (match to HOIPKO)	Synthego-ATCC	
HOIPKO THP1	This paper (Synthego)	
ATG16L1KO THP1	This paper (Synthego)	
Recombinant DNA		
pSpCas9(BB)-2A-Puro (PX459) V2.0	Addgene	#62988
pLKO.1	Addgene	#8453
pTRIP_BFP-P2A-STING	Addgene	#102597
pHAGEb_mEGFP-LC3B	This paper	
pHAGEb_mEGFP-HOIP	This paper	
pHAGEb_HOIP_IRES_mCh-3xNLS	This paper	
pHAGEb_mScar-LC3B	This paper	
pHAGEb_mEGFP-OTULIN	This paper	
pHAGEb_mEGFP-SopF	This paper and Fischer et al., 2020	
Antibodies		
Ms Mono- and Polyubiquitinated conjugates (UBCJ2)	Enzo	ENZ-ABS840
Ms Anti-STING (OTI4HI)	Thermo Scientific	MA5-26030
Rb Anti-STING/TMEM173	Novus	NBP2-24683
Anti-Ubiquitin, Clone VU-1	Life Sensors	VU-0101
Rb Anti-Ubiquitin, K48-Specific, Clone Apu2	Millipore Sigma	ZRB2150
Rb Anti-Ubiquitin, Lys63-specific, Clone Apu3	Millipore Sigma	05-1308
Rb Anti-Linear Ubiquitin, clone 1E3 ZooMab	Sigma-Aldrich	ZRB2114
Rb Anti-GAPDH	Sigma-Aldrich	G9545
Rb Anti-HOIP/RNF31, E6M5B	CST	99633S
Rb Anti-RNF31	Fortis Life Sciences	A303-560A-T

Rb Anti-Ranbp-Type and C3Hc4-Type Zinc Finger Containing 1 (HOIL-1)	Proteintech	26367-1-AP
Rb Anti-SHARPIN	Proteintech	14626-1-AP
Rb Anti-LC3B	Sigma-Aldrich	L7543
Rb Anti-phospho-STING(S366), D7C3S	CST	19781s
Rb Anti-STING(D2P2F)	CST	13647
Rb Anti-HSP90(a/b), H-114	SCBT	sc-7947
Rb Anti-TNFAIP3-Interacting Protein 1 (TNIP1)	Proteintech	15104-1-AP
Rb Anti-OPTN	Proteintech	10837-I-AP
Rb Anti-IkBa, 44D4	CST	4812S
Rb Anti-phospho-IkBa(S32), 14D4	CST	2859S
Rb Anti-NFkB p65 (D14E12) XP	CST	8242
Rb Anti-phospho-NFkB p65 (S536) (93H1)	CST	3033
Rb Anti-TBK1/NAK	CST	3013
Rb phospho-TBK1/NAK(S172) (D52C2) XP	CST	5483
Rb Anti-IRF3 (D83B9)	CST	4302
pIRF3(S386)	Abcam	ab76493
Rb Anti-Vinculin (E1E9V) XP	CST	13901S
Ms Anti-Actin, Clone C4	Sigma-Aldrich	MAB1501
Goat Anti-Rabbit IgG (H+L) Cross-Adsorbed, Alexa Fluor 647	Invitrogen	A-21244
Goat Anti-Mouse IgG (H+L) Cross-Adsorbed, Alexa Fluor 647	Invitrogen	A-21235
Goat Anti-Rabbit IgG (H+L) Cross-Adsorbed, Alexa Fluor 546	Invitrogen	A-11035
Goat Anti-Mouse IgG (H+L) Cross-Adsorbed, Alexa Fluor 546	Invitrogen	A-11003
Rabbit IgG, HRP-Linked F(ab') ₂ Fragment, Donkey	Cytiva	NA9340
Mouse IgG, HRP-Linked F(ab') ₂ Fragment, Sheep	Cytiva	NA9310
Oligonucleotides and other sequence-based reagents		
qPCR primers sequences	This paper	Table 1
CRISPR gRNA sequences	This paper	Table 2
shRNA Target sequences	This paper	Table 3
Chemicals, Enzymes and other reagents		
2'3' cGAMP Sodium Salt	Chemietek	CT-CGMAP
Monensin sodium salt, 90-95%(TLC)	Sigma-Aldrich	M5273
TNFa	Peptotech	300-01A
diABZI STING agonist-1 (trihydrochloride)	MedChem Express	HY-112921B
diABZI STING agonist (Compound 3)	Selleck Chemicals	S8796
STING agonist C53	Tocris	7741
Puromycin	Invivogen	ant-pr-1
Saponin	Sigma-Aldrich	47036
Shield1	TakaraBio	632189
Doxycycline	Sigma-Aldrich	D3447
Quick-RNA MiniPrep Plus kit	Zymo Research	R1058
High-Capacity cDNA Reverse Transcription Kit	Thermo Scientific	4368814
PowerUp SYBR Green Master Mix	Thermo Scientific	A25742

Control Magnetic Beads (negative control)	Lifesensors	UM-400M-1000
TUBE 1 (High capacity magnetic beads)	Lifesensors	UM501M
Hoeschst	Thermo Scientific	H1399
Jetoptimus	Polyplus	101000006
NEBuilder HiFi DNA Assembly Cloning Kit, with Competent Cells	New England Biolabs	E5520S
DMEM	Thermofisher	#31053028
Fetal Bovine Serum - Premium Select, Heat inactivated	R&D	S11550H
Sodium Pyruvate	Thermofisher	#11360070
GlutaMAX	Thermofisher	#35050061
RPMI (ATCC modification)	ATCC	30-2001
OptiMEM	Gibco	31985062
Software		
Zen	Zeiss	
ImageLab	BioRad	
FIJI	Schindelin et al., 2012	
Prism	GraphPad	
Other		
8 well chambered coverglass with #1.5 high performance coverglass	Cellvis	C8-1.5H-N
96-well glass bottom plates	DOT Scientific Inc	MGB096-12-LG-L
Surepage 4-12% Bis-Tris gels, 10-, 12-, 15-well	Genscript	
Nupage 4-12% Bis-Tris gels, 20 well	Thermo Scientific	WG1402
Nupage 3-8% Tris-Acetate gels, 1.0 mm, 15 well	Thermo Scientific	EA03755
S-Trap Columns	Protifi	C02-micro

Table 1. qPCR Primer Sequences

Gene	F/R Primer Sequences
Hu <i>IFNB1</i>	F: CTTGGATTCCTACAAAGAAGCAGC R: TCCTCCTTCTGGAACTGCTGCA
Hu <i>IFIT3</i>	F: CGGAACAGCAGAGACACAGA R: CGGAACAGCAGAGACACAGA
Hu <i>ISG15</i>	F: TGAGAGGCAGCGAACTCATC R: CAGCATCTTCACCGTCAGGT
Hu <i>TNF</i>	F: CTCTTCTGCCTGCTGCACTTTG R: ATGGGCTACAGGCTTGCTACTC
Hu <i>TNFAIP3</i>	F: GAAGCTTGTGGCGCTGAAAA R: GAACGCCCCACATGTACTGA
Hu <i>IL6</i>	F: AAGCCAGAGCTGTGCAGATG R: GCATTTGTGGTTGGGTCAGG
Hu <i>ACTB</i>	F: GCACTCTTCCAGCCTTCCTT R: AATGCCAGGGTACATGGTGG

Ms <i>IFNB1</i>	F: GCCTTTGCCATCCAAGAGATGC
	R: ACACTGTCTGCTGGTGGAGTTC
Ms <i>IFIT3</i>	F: GCTCAGGCTTACGTTGACAAGG
	R: CTGCAAGTGCATCATCGTTGTTC
Ms <i>ISG15</i>	F: CATCCTGGTGAGGAACGAAAGG
	R: CTCAGCCAGAACTGGTCTTCGT
Ms <i>TNF</i>	F: GGTGCCTATGTCTCAGCCTCTT
	R: GCCATAGAACTGATGAGAGGGAG
Ms <i>TNFAIP3</i>	F: AGCAAGTGCAGGAAAGCTGGCT
	R: GCTTTCGCAGAGGCAGTAACAG
Ms <i>IL6</i>	F: TACCACTTCACAAGTCGGAGGC
	R: CTGCAAGTGCATCATCGTTGTTC
Ms <i>ACTB</i>	F: CATTGCTGACAGGATGCAGAAGG
	R: TGCTGGAAGGTGGACAGTGAGG

Table 2. CRISPR gRNA Information

Cell Line	Gene	gRNA	Transcript ID	Exon
HOIPKO HeLa	<i>RNF31</i>	(5'-GAATACTCATCCAAGACAGC-3')	ENST00000324103.11	Exon 4
		(3'-GCTGTCTTGGATGAGTATTC-5')		
HOIPKO ^{pool} THP1	<i>RNF31</i>	UGCAGGUAGCGGGCGGCUAG	ENST00000324103.11	Exon 1
		CCUGAGGAGGGAUUCCGGGC		
		CAGGAUGCCGGGGGAGGAAG		
ATG16L1KO THP1	<i>ATG16L1</i>	GACAAUGUGGAUACUCAUCC	ENST00000392018.1	Exon 10

Table 3. shRNA Target Information

Cell Line	shRNA target sequence	Gene	Transcript ID
shHOIP iBMDMs	GCCACTATTCGCTACCTACAT	<i>RNF31</i>	ENSMUST00000019443.15

Methods and Protocols

Cell Culture

HeLa (ATCC), HeLa FRT/TREX, HEK293T (ATCC), and immortalized mouse bone marrow derived macrophage (iBMDM) cells were cultured in Dulbecco's Modified Eagle Medium (DMEM; ThermoFisher) supplemented with 10% (v/v) Fetal Bovine Serum (FBS; R&D), 1 mM Sodium Pyruvate (ThermoFisher), and 2 mM GlutaMAX (ThermoFisher). THP1 (Synthego-ATCC) cells were cultured in Roswell Park Memorial Institute (RPMI) 1640 (ATCC). HeLa FRT/TREX cells stably expressing an inducible version of the Vx3-EGFP sensor

previously reported in (Sims *et al*, 2012) with a DD degron fused to the N-terminus (pcDNA5-FRT/TO-DD-Vx3-EGFP) were kindly provided by Tingting Yao and Robert Cohen. iBMDMs were kindly shared by Howard Young and previously reported in (Blasi *et al*, 1987, 1989).

Cloning and Generation of Stable Cell Lines

pHAGEb vectors were modified from the pHAGE (HIV-1 Gustavo George Enhanced) vector. Plasmids were generated by PCR amplification of open reading frames (ORFs) in cDNA and ligation into a linearized pHAGEb vector using a Gibson assembly kit (New England Biolabs). dh5a or Stable competent *E. coli* cells (New England Biolabs) were then transformed with assembled plasmids and grown on LB agar plates with appropriate antibiotics. Single colonies were selected, expanded in antibiotic containing liquid culture, and screened for successful insertion of the amplicon by diagnostic restriction enzyme digest. Selected plasmids were further validated by sanger sequencing. Complete plasmid sequences are available upon request.

HeLa cell lines with stable overexpression of indicated genes were generated by lentivirus infection. Lentivirus was generated using HEK293T cells and lentiviral system plasmids (pHDM-G, pHDM-HGPM2, pHDM-tat1B, and pRC-CMV-rev1B) using a protocol detailed in Wang, 2020 (Wang, 2020). HEK293T cells were transfected with the lentiviral system plasmids (500ng each), plasmid DNA (1ug) and PEI prepared in OptiMEM media (Gibco). Following an initial exchange for fresh media 16-24 hours after transfection, lentiviral conditioned media was harvested 28-72 hours post-transfection and filtered through a 0.45um PVDF syringe filter prior to transduction of target cells. Target cells were transduced by incubating cells with generated lentivirus and 8 ug/mL Polybrene for 24 hours. At least three days following transduction, generated stable cell lines were sorted based on the expressed fluorescent proteins using Fluorescence-Activated Cell Sorting (FACS) to obtain homogenous cell populations at empirically determined optimal protein expression.

Generation of CRISPR Knockout Cell Lines

For HOIPKO HeLa cells, gRNAs were annealed and ligated into a BbsI-digested pSpCas9(BB)-2A-Puro (PX459) V2.0 vector (Addgene #62988). Assembled plasmid DNA was expanded as described above. HeLa cells were transfected with the gRNA-containing plasmid using the JetOptimus (Polyplus) transfection reagent, and subsequently treated with 1 ug/ml puromycin (Invivogen) for 2 days to select for cells expressing

the plasmid. Isolation of single cells from the puromycin-resistant pool was obtained by limiting dilution and clonal expansion in 96 well plates. Individual clones were then screened for knockout edits by PCR amplification of the target locus from extracted genomic DNA and sanger sequencing of the amplicon. Sequence data was analyzed using the Inference of CRISPR Edits (ICE) tool from Synthego to identify clones with frame-shifting insertions or deletions (InDels). Selected clones were finally validated by measuring protein abundance detected by immunoblotting. HOIPKO HeLa cells are from Fischer et al., 2020. HOIPKO and ATG16L1KO THP1 and Mock transfected WT cells were purchased as an express pooled cell line from Synthego. Details for gRNA sequences for each KO cell line are in Supplemental File 1.

shRNA Knockdown Cell Lines

For shHOIP cells, target shRNA sequence for mouse RNF31 (Supplemental File 1) was adapted, annealed, and ligated into EcoRI and AgeI-digested pLKO.1 vector as per the Addgene protocol (addgene: #8453). Assembled plasmid DNA was expanded, and lentivirus was produced as described above for both the shRNA target containing vector (shHOIP) and an empty vector (shCtrl). iBMDMs were incubated with viral inoculum for seven hours. Seventy-two hours after removal of viral inoculum, cells were treated with 10ug/mL puromycin for six days, and then validated for knockdown at the protein level by immunoblotting.

Cell treatment with STING agonists

For treatments of different STING agonists (cGAMP, diABZI, and C53), 12-24 hours following cell plating for each experiment (more details below), cell culture medium was replaced, and agonists were added to the fresh medium. No transfection or permeabilization reagents were used.

Immunofluorescence

Cells were plated onto #1.5 chambered coverglass (Cellvis) or in 96 well glass plates (DOT Scientific Inc) 18-24 hours before experiments were performed. Following indicated treatments, cells were fixed with prewarmed 4% paraformaldehyde (PFA; Electron Microscopy Services) for 10-15 minutes at 37°C. For general immunofluorescence procedures, fixed cells were rinsed with 1xPBS and permeabilized with 0.5% Triton-X 100 (Sigma) in 1xPBS for 5 minutes prior to blocking for 1 hour in buffer containing 3% goat serum, 1% BSA, and

0.1% Tween-20 in 1xPBS. Cells were then incubated with primary antibody prepared in blocking buffer overnight at 4°C and then washed with 1xPBS prior to incubation with secondary antibodies in blocking buffer for 1 hour at room temperature.

For linkage-specific ubiquitin antibodies, cells were incubated in blocking buffer overnight at 4°C, and then incubated in primary antibodies prepared in blocking buffer for 1 hour at room temperature prior to the washing and secondary antibody incubation steps per the recommended protocol described in Newton *et al.*, 2012 (Newton *et al.*, 2012). Following immunostaining, cells were stained with Hoechst dye prior to imaging.

For saponin extraction, cells were rinsed with ice cold HBSS, permeabilized with Saponin Extraction Buffer (SEB; 80mM PIPES, pH 6.8, 1mM MgCl₂, 1mM EGTA, 0.1% Saponin (w/v)) for 2 minutes, then 4 minutes on ice, and washed again 2x with HBSS prior to fixation as described above (Tarantino *et al.*, 2014).

Live Cell Imaging

For live cell imaging, cells were plated in 96 well glass plates (DOT Scientific Inc) 18-24 hours before experiments were performed. For Vx3-EGFP (K63-Ub Sensor) cells were treated with Doxycycline (1 ug/mL) and the Shield1 ligand (500nM) at the time of plating and at least 24 hours prior to experiments. Image acquisition began immediately after indicated treatments and occurred every 30 minutes over a 12-hour time course. Imaging was performed in a live-cell chamber at 37°C, 5% CO₂, and constant humidity.

Microscopy

For super-resolution imaging, fixed and/or immunostained cells were imaged on a Zeiss LSM 880 Airyscan Confocal Microscope using a Zeiss 63x 1.4 NA Plan-Apochromat objective, equipped with a Piezo high-precision stage at room temperature. Z-stack images were acquired with 405-, 488-, 561-, and 633-nm lasers, MBS 488/561/633 and MBS 405 beam splitters, Zeiss BP 570-620 + LP 645, BP 420-480 + BP 495-550, and BP 420-480 + LP 605 emission filters, and the Airyscan detector in frame scan mode using the Zen software platform (Carl Zeiss Microscopy). Images were then processed for Airyscan 3D deconvolution using Zen software and prepared for publication using FIJI open-source software (Schindelin *et al.*, 2012). Upper limits of the pixel display range were adjusted to improve brightness in representative images.

For quantitative and live cell imaging, fixed and immunostained cells, or live cells were imaged on a Nikon Ti-2 CSU-W1 spinning disk confocal microscope using a 40x 1.15 NA water objective, equipped with an automated TI2-N-WID water immersion dispenser. Images were acquired with 405-, 488-, 561-, and 633-nm lasers and 698/70 nm emission filter using the Nikon elements AR microscope imaging software.

Image Analysis

For Pearson Correlation Coefficient analysis, custom MATLAB scripts were used that performed automated background subtraction and cell segmentation by intensity and size. Individual cells were segmented by performing a gaussian blur on the LC3B channel, then performing a watershedding algorithm to separate the blurred peaks. The separating lines from watershedding were then imposed on the cell mask to separate connected components to isolate single cells. The Pearson's Correlation Coefficient was calculated for the pixels within each cell, then the median value found for each image. The median value was calculated between each image taken for each well of a 96 well plate, and then averages and standard deviations calculated between wells.

For percent cells with foci, custom MATLAB scripts performed similar processing and cell segmentation to the Pearson's Correlation analysis, but a secondary segmentation for punctate structures was performed. To find punctae and foci, cell-sized regions were equalized by dividing the image by a gaussian blur of the image, then pixels with high intensity in both the original image and the equalized image found and filtered by size and, in some cases, circularity. The number of pixels positive in the foci mask were then counted for each connected component in the segmented single cell mask and, if above a threshold, were considered cells positive for foci.

For percent foci positive for ubiquitin, we used custom MATLAB scripts to identify LC3B foci as above, then treated each as individual connected components in a loop. Each component underwent a morphological dilation, and the original mask subtracted to generate a 'donut' shape with no overlapping foci. Then a ratio was found between the foci component and the corresponding dilation to find if there is a higher intensity in the foci compared to near the foci. Foci with a ratio greater than the threshold 1.75 were considered positive for ubiquitin or a specific ubiquitin chain for which they were stained. All MATLAB scripts are available upon request. Please see schematic in Appendix Figure S2 for MATLAB workflow.

Immunoblotting

Cells were plated in 12-well or 6-well plates 18-24 hours prior to experiments. Following indicated treatments, cells were washed with ice cold HBSS, lysed in ice cold 1x LDS sample buffer (Genscript) supplemented with cComplete Protease Inhibitor cocktail (Roche), and boiled immediately at 99°C for 10 minutes. Protein quantitation per sample was obtained using Pierce BCA protein assay kit (ThermoFisher). Dithiothreitol (DTT; Sigma) was added to each sample at a final concentration of 100 mM just before gel loading.

For general immunoblotting procedures, 20-30ug of total protein per sample was loaded into wells of 4-12% Bis-Tris gels (Genscript or Invitrogen) and separated in MES or MOPS buffer ran at 65v for 30 minutes, then 125v until the dye front reached the bottom of the gel. Separated proteins were then transferred onto 0.45 um Nitrocellulose membranes in BioRad Transblot Turbo Transfer Buffer with 20% EtOH using the Biorad Trans-Blot Turbo Transfer system (semi-dry). Membranes were blocked in 5% milk 1xPBST at room temperature (RT) for 1 hour prior to primary antibody incubation in 3% BSA 1xPBST at 4°C overnight. Membranes were then thoroughly washed in PBST, incubated in HRP conjugated secondary antibodies raised against the appropriate species in 5% milk PBST for 1 hour at room temperature, and finally washed. HRP signal was developed using either Amersham ECL Prime (Cytiva) or SuperSignal West Femto ECL (Thermo Scientific) and detected using a ChemiDoc Imaging System (BioRad). Images were analyzed using ImageLab (BioRad).

For detection of linkage-specific ubiquitin, a modified version of the protocol described in Newton et al., 2012 (Newton *et al*, 2012) was used. 10-15ug total protein was loaded into wells of 3-8% Tris-Acetate gels and separated in tris acetate buffer (Invitrogen) ran at 65v for 30 minutes and then 125v until the dye front reached the bottom of the gel. Separated proteins were then transferred onto 0.45um a Nitrocellulose membrane at 30v for 2 hours in Tris-Glycine buffer (Towbin formulation) supplemented with 10% MeOH using the XCell SureLock blot module system (semi-wet). Membranes were blocked in 5% milk 1xPBST overnight at 4°C, then incubated in primary antibodies in 5% milk 1xPBST for 1 hour at room temperature. Membranes were then thoroughly washed in PBST, incubated in HRP conjugated secondary antibodies raised against the appropriate species in

5% milk PBST for 1 hour at room temperature, and finally washed. HRP signal was developed using SuperSignal West Femto ECL and detected and analyzed as described above.

For quantification of immunoblots, raw images were analyzed using ImageLab (BioRad) to detect band volume or lane volume (phosho and Ub blots). All band or lane values were normalized to the corresponding internal loading control (GAPDH, Vinculin, or HSP90). Relative values were then calculated as indicated in the figures and plotted using Prism 9.

LC-MS/MS Quantification of Ubiquitin Linkages

HeLa cells were plated in a 15cm dish ~48 hours prior to experiments. Following treatment, cells were washed 2x with ice cold 1xPBS supplemented with N-Ethymaleimide (NEM; 5mM), scraped from the dish, and centrifuged at 2,000xg for 2 minutes at 4°C. Supernatant was removed, and the cell pellets were resuspended in ice cold lysis buffer (50mM Tris-HCl, pH 7.5, 150mM NaCl, 1% NP-40, 1mM EDTA, 10% Glycerol) supplemented with the deubiquitylase and protease inhibitors (100uM PR-619, 5mM O-Phelanthroline, 5mM NEM, and cOmplete protease inhibitor cocktail). For preparation of peptides from cell lysates, a modified protocol for S-Trap spin column digestion from Protifi was used. ~40ug of protein from the cell lysates was solubilized in either a mixture of 5% SDS, 8M Urea, and 100mM TEAB or 10% SDS and 100mM TEAB, and mixed at 50oC for 5 minutes. After solubilization, samples were reduced with 0.1M TCEP for 15 minutes at room temperature, then alkylated with 0.22M NEM for 15 minutes at room temperature in the dark. Samples were then acidified with 12-21% aqueous phosphoric acid prior to digestion with Trypsin/Lys-C (Promega) and then added immediately to an S-Trap column (Protifi) loaded with S-Trap binding buffer (90% MeOH and 100mM TEAB). Following an initial centrifugation at 4,000xg to trap the proteins, the column was washed with S-Trap Binding Buffer, and then either incubated overnight at 37°C or for 2 hours at 47oC in digestion buffer (Trypsin-LysC and 50mM TEAB) for complete protein digestion. After digestion, the column was rehydrated with 50mM TEAB, and digested peptides were eluted with 0.2% aqueous formic acid, and then a mixture of 0.2% aqueous formic acid and 50% acetonitrile. Peptides eluted from the S-Trap were dried under vacuum and stored at -20oC until analysis. For analysis, each sample was resuspended in 0.1% TFA, a nanodrop reading was taken at UV280 to normalize loading. NanoLC-MS/MS analysis of tryptic peptides was carried out with a Thermo Scientific Fusion Lumos tribrid mass spectrometer interfaced to a UltiMate3000 RSLCnano HPLC

system (Thermo Scientific). For each analysis, ~1 μg of the tryptic digest was loaded and desalted in an Acclaim PepMap 100 trapping column (75 μm , 2 cm) at 4 $\mu\text{L}/\text{min}$ for 5 min. Peptides were then eluted into an Thermo Scientific Acclaim PepMap™ 100 column, (3 μm , 100 \AA , 75 $\mu\text{m} \times 250 \text{ mm}$) and chromatographically separated using a binary solvent system consisting of A: 0.1% formic acid and B: 0.1% formic acid and 80% acetonitrile at a flow rate of 300 nL/min. A gradient was run from 5% B to 37.5%B over 60 minutes, followed by a 5-minute wash step with 90% B and 10-minute equilibration at 5% B before the next sample was injected. The orbitrap Lumos mass spectrometer operated in unscheduled Parallel Reaction Monitor (PRM) mode. Precursor masses were detected in the Orbitrap at $R=120,000$ (m/z 200). Charge state with the strongest signal of each ubiquitylated ubiquitin peptide was added to the target list. Isolation window was 1.2 m/z . MS/MS spectra were acquired in the orbitrap with $R= 30,000$ (m/z 200), with AGC target 500%. Collision energy was 28%. Data was processed using Skyline (MacLean *et al*, 2010) for quantification. Peak detection and integration were manually validated for each peptide before quantification results were exported to Excel.

Quantitative Real-Time PCR

Total RNA from $5\text{-}10 \times 10^5$ cells was extracted using Quick-RNA MiniPrep Plus kit (Zymo Research) followed by reverse transcription using High-Capacity cDNA Reverse Transcription Kit (Thermo Fisher Scientific). Equal amounts of cDNA and corresponding primers were used for qPCR using SYBR Green Master Mix (Thermo Fisher Scientific) and a CFX384 real-time system/C100 Touch Thermal Cycler (Bio-Rad). For each biological sample, the Ct value of the gene interested was normalized against the b-actin Ct to calculate ΔCt . Each ΔCt was normalized to the average ΔCt of untreated samples to generate the $\Delta\Delta\text{Ct}$ value. Relative gene expression was then analyzed using the $2^{-\Delta\Delta\text{Ct}}$ formula and plotted in figures (Livak & Schmittgen, 2001). Details for PCR primers can be found in Supplemental File 1.

Statistics

For quantitative RT-PCR, one way or 2-way ANOVA was performed on the $2^{-\Delta\Delta\text{Ct}}$ values with a Tukey's multiple comparisons test. Statistical analyses were performed using Prism (GraphPad).

Acknowledgements

We would like to thank the NHLBI Flow Cytometry Core, the NINDS Light Microscopy Core, and the NIDCR Mass Spectrometry Facility (ZIA DE00075) for excellent assistance. We would like to thank Howard Young, NIH Scientist Emeritus at NCI and the immunology community at NIH for sharing resources and insights on NF κ B signaling. We would also like to thank the Youle lab members for feedback and helpful discussions.

Funding

Intramural Research Program (IRP) of the National Institute of Neurological Disorders and Stroke (NINDS; RJY) and the National Institute of Dental and Craniofacial Research (NIDCR; AW).

Author Contributions

Conceptualization: TDF, RJY

Methodology: TDF, FLG, ENB, PPZ, AW, YW, TY, FS, RC

Investigation: TDF, ENB, PPZ, EDM

Visualization: TDF, ENB

Funding acquisition: RJY, AW

Project administration: TDF, RJY

Writing – original draft: TDF, RJY

Writing – review & editing: TDF, FLG, ENB, PPZ, EDM, AW, YW, RJY, TY, FS, RC

Disclosure and Competing Interests

The authors declare no competing interests.

Data and Materials Availability

All cell lines and plasmids are available upon request and materials transfer agreement. MATLAB codes are available upon request.

- MS data:

MassIVE [MSV000092940](https://massive.ucsd.edu/ProteoSAFe/private-dataset.jsp?task=00ef1e46d6814baca9fcc1a2f479b012) (<https://massive.ucsd.edu/ProteoSAFe/private-dataset.jsp?task=00ef1e46d6814baca9fcc1a2f479b012>)

References

- Abe T & Barber GN (2014) Cytosolic-DNA-Mediated, STING-Dependent Proinflammatory Gene Induction Necessitates Canonical NF- κ B Activation through TBK1. *J Virol* 88: 5328–5341
- Ablasser A & Chen ZJ (2019) cGAS in action: Expanding roles in immunity and inflammation. *Science* 363: eaat8657
- Ahn J & Barber GN (2019) STING signaling and host defense against microbial infection. *Exp Mol Med* 51: 1–10
- Balka KR, Louis C, Saunders TL, Smith AM, Calleja DJ, D’Silva DB, Moghaddas F, Tailleur M, Lawlor KE, Zhan Y, *et al* (2020) TBK1 and IKK ϵ Act Redundantly to Mediate STING-Induced NF- κ B Responses in Myeloid Cells. *Cell Reports* 31
- Blasi E, Radzioch D, Durum SK & Varesio L (1987) A murine macrophage cell line, immortalized by v-raf and v-myc oncogenes, exhibits normal macrophage functions. *Eur J Immunol* 17: 1491–1498
- Blasi E, Radzioch D, Merletti L & Varesio L (1989) Generation of macrophage cell line from fresh bone marrow cells with a myc/raf recombinant retrovirus. *Cancer Biochem Biophys* 10: 303–317
- Chen Q, Sun L & Chen ZJ (2016) Regulation and function of the cGAS-STING pathway of cytosolic DNA sensing. *Nat Immunol* 17: 1142–9
- Dobbs N, Burnaevskiy N, Chen D, Gonugunta VK, Alto NM & Yan N (2015) STING Activation by Translocation from the ER Is Associated with Infection and Autoinflammatory Disease. *Cell Host Microbe* 18: 157–68
- Emmerich CH, Ordureau A, Strickson S, Arthur JSC, Pedrioli PGA, Komander D & Cohen P (2013) Activation of the canonical IKK complex by K63/M1-linked hybrid ubiquitin chains. *Proceedings of the National Academy of Sciences* 110: 15247–15252
- Fiil BK, Damgaard RB, Wagner SA, Keusekotten K, Fritsch M, Bekker-Jensen S, Mailand N, Choudhary C, Komander D & Gyrd-Hansen M (2013) OTULIN Restricts Met1-Linked Ubiquitination to Control Innate Immune Signaling. *Molecular Cell* 50: 818–830
- Fischer TD, Wang C, Padman BS, Lazarou M & Youle RJ (2020) STING induces LC3B lipidation onto single-membrane vesicles via the V-ATPase and ATG16L1-WD40 domain. *J Cell Biol* 219
- Gentili M, Liu B, Papanastasiou M, Dele-Oni D, Schwartz MA, Carlson RJ, Al’Khafaji AM, Krug K, Brown A, Doench JG, *et al* (2023) ESCRT-dependent STING degradation inhibits steady-state and cGAMP-induced signalling. *Nat Commun* 14: 611
- Gui X, Yang H, Li T, Tan X, Shi P, Li M, Du F & Chen ZJ (2019) Autophagy induction via STING trafficking is a primordial function of the cGAS pathway. *Nature* 567: 262–266
- Haas TL, Emmerich CH, Gerlach B, Schmukle AC, Cordier SM, Rieser E, Feltham R, Vince J, Warnken U, Wenger T, *et al* (2009) Recruitment of the Linear Ubiquitin Chain Assembly Complex Stabilizes the

- TNF-R1 Signaling Complex and Is Required for TNF-Mediated Gene Induction. *Molecular Cell* 36: 831–844
- Hopfner KP & Hornung V (2020) Molecular mechanisms and cellular functions of cGAS-STING signalling. *Nat Rev Mol Cell Biol* 21: 501–521
- Ishikawa H & Barber GN (2008) STING is an endoplasmic reticulum adaptor that facilitates innate immune signalling. *Nature* 455: 674–8
- Ishikawa H, Ma Z & Barber GN (2009) STING regulates intracellular DNA-mediated, type I interferon-dependent innate immunity. *Nature* 461: 788–92
- Jacquin E, Leclerc-Mercier S, Judon C, Blanchard E, Fraitag S & Florey O (2017) Pharmacological modulators of autophagy activate a parallel noncanonical pathway driving unconventional LC3 lipidation. *Autophagy* 13: 854–867
- Keusekotten K, Elliott PR, Glockner L, Fiil BK, Damgaard RB, Kulathu Y, Wauer T, Hospenthal MK, Gyrd-Hansen M, Krappmann D, *et al* (2013) OTULIN Antagonizes LUBAC Signaling by Specifically Hydrolyzing Met1-Linked Polyubiquitin. *Cell* 153: 1312–1326
- Kirisako T, Kamei K, Murata S, Kato M, Fukumoto H, Kanie M, Sano S, Tokunaga F, Tanaka K & Iwai K (2006) A ubiquitin ligase complex assembles linear polyubiquitin chains. *The EMBO Journal* 25: 4877–4887
- Komander D & Rape M (2012) The ubiquitin code. *Annu Rev Biochem* 81: 203–29
- Kuchitsu Y, Mukai K, Uematsu R, Takaada Y, Shinojima A, Shindo R, Shoji T, Hamano S, Ogawa E, Sato R, *et al* (2023) STING signalling is terminated through ESCRT-dependent microautophagy of vesicles originating from recycling endosomes. *Nat Cell Biol* 25: 453–466
- Landau LM, Chaudhary N, Tien YC, Rogozinska M, Joshi S, Yao C, Crowley J, Hullahalli K, Campbell IW, Waldor MK, *et al* (2024) pLxIS-containing domains are biochemically flexible regulators of interferons and metabolism. *Mol Cell* 84: 2436-2454.e10
- Liu B, Carlson RJ, Pires IS, Gentili M, Feng E, Hellier Q, Schwartz MA, Blainey PC, Irvine DJ & Hacohen N (2023) Human STING is a proton channel. *Science* 381: 508–514
- Livak KJ & Schmittgen TD (2001) Analysis of Relative Gene Expression Data Using Real-Time Quantitative PCR and the 2- $\Delta\Delta$ CT Method. *Methods* 25: 402–408
- MacLean B, Tomazela DM, Shulman N, Chambers M, Finney GL, Frewen B, Kern R, Tabb DL, Liebler DC & MacCoss MJ (2010) Skyline: an open source document editor for creating and analyzing targeted proteomics experiments. *Bioinformatics* 26: 966–968
- Mann CC de O, Orzalli MH, King DS, Kagan JC, Lee ASY & Kranzusch PJ (2019) Modular Architecture of the STING C-Terminal Tail Allows Interferon and NF- κ B Signaling Adaptation. *Cell Reports* 27: 1165-1175.e5
- Matsumoto ML, Dong KC, Yu C, Phu L, Gao X, Hannoush RN, Hymowitz SG, Kirkpatrick DS, Dixit VM & Kelley RF (2012) Engineering and Structural Characterization of a Linear Polyubiquitin-Specific Antibody. *Journal of Molecular Biology* 418: 134–144
- Mizushima N (2020) The ATG conjugation systems in autophagy. *Current Opinion in Cell Biology* 63: 1–10
- Newton K, Matsumoto ML, Ferrando RE, Wickliffe KE, Rape M, Kelley RF & Dixit VM (2012) Using Linkage-Specific Monoclonal Antibodies to Analyze Cellular Ubiquitylation. In *Ubiquitin Family Modifiers and the*

Proteasome: Reviews and Protocols, Dohmen RJ & Scheffner M (eds) pp 185–196. Totowa, NJ: Humana Press

- Ni G, Konno H & Barber GN (2017) Ubiquitination of STING at lysine 224 controls IRF3 activation. *Science Immunology* 2: eaah7119
- Prabakaran T, Bodda C, Krapp C, Zhang BC, Christensen MH, Sun C, Reinert L, Cai Y, Jensen SB, Skouboe MK, *et al* (2018) Attenuation of cGAS-STING signaling is mediated by a p62/SQSTM1-dependent autophagy pathway activated by TBK1. *Embo j* 37
- Pryde DC, Middya S, Banerjee M, Shrivastava R, Basu S, Ghosh R, Yadav DB & Surya A (2021) The discovery of potent small molecule activators of human STING. *Eur J Med Chem* 209: 112869
- Rahighi S, Ikeda F, Kawasaki M, Akutsu M, Suzuki N, Kato R, Kensche T, Uejima T, Bloor S, Komander D, *et al* (2009) Specific Recognition of Linear Ubiquitin Chains by NEMO Is Important for NF- κ B Activation. *Cell* 136: 1098–1109
- Ruland J (2011) Return to homeostasis: downregulation of NF- κ B responses. *Nat Immunol* 12: 709–714
- Sasaki K & Iwai K (2015) Roles of linear ubiquitinylation, a crucial regulator of NF- κ B and cell death, in the immune system. *Immunological Reviews* 266: 175–189
- Schindelin J, Arganda-Carreras I, Frise E, Kaynig V, Longair M, Pietzsch T, Preibisch S, Rueden C, Saalfeld S, Schmid B, *et al* (2012) Fiji: an open-source platform for biological-image analysis. *Nat Methods* 9: 676–82
- Sims JJ, Scavone F, Cooper EM, Kane LA, Youle RJ, Boeke JD & Cohen RE (2012) Polyubiquitin-sensor proteins reveal localization and linkage-type dependence of cellular ubiquitin signaling. *Nat Methods* 9: 303–9
- Takahashi M, Lio C-WJ, Campeau A, Steger M, Ay F, Mann M, Gonzalez DJ, Jain M & Sharma S (2021) The tumor suppressor kinase DAPK3 drives tumor-intrinsic immunity through the STING-IFN- β pathway. *Nat Immunol* 22: 485–496
- Tan Y & Kagan JC (2019) Innate Immune Signaling Organelles Display Natural and Programmable Signaling Flexibility. *Cell* 177: 384-398.e11
- Tarantino N, Tinevez J-Y, Crowell EF, Boisson B, Henriques R, Mhlanga M, Agou F, Israël A & Laplantine E (2014) TNF and IL-1 exhibit distinct ubiquitin requirements for inducing NEMO–IKK supramolecular structures. *Journal of Cell Biology* 204: 231–245
- Tokunaga F, Sakata S, Saeki Y, Satomi Y, Kirisako T, Kamei K, Nakagawa T, Kato M, Murata S, Yamaoka S, *et al* (2009) Involvement of linear polyubiquitylation of NEMO in NF- κ B activation. *Nat Cell Biol* 11: 123–132
- Tsuchida T, Zou J, Saitoh T, Kumar H, Abe T, Matsuura Y, Kawai T & Akira S (2010) The ubiquitin ligase TRIM56 regulates innate immune responses to intracellular double-stranded DNA. *Immunity* 33: 765–76
- Wang C (2020) A Sensitive and Quantitative mKeima Assay for Mitophagy via FACS. *Current Protocols in Cell Biology* 86: e99
- Xu Y, Cheng S, Zeng H, Zhou P, Ma Y, Li L, Liu X, Shao F & Ding J (2022) ARF GTPases activate Salmonella effector SopF to ADP-ribosylate host V-ATPase and inhibit endomembrane damage-induced autophagy. *Nat Struct Mol Biol* 29: 67–77

- Xu Y, Zhou P, Cheng S, Lu Q, Nowak K, Hopp A-K, Li L, Shi X, Zhou Z, Gao W, *et al* (2019) A Bacterial Effector Reveals the V-ATPase-ATG16L1 Axis that Initiates Xenophagy. *Cell* 178: 552-566.e20
- Xun J, Zhang Z, Lyu B, Lu D, Yang H, Shang G & Tan JX (2023) A conserved ion channel function of STING mediates non-canonical autophagy and cell death. 2023.08.26.554976 doi:10.1101/2023.08.26.554976 [PREPRINT]
- Yum S, Li M, Fang Y & Chen ZJ (2021) TBK1 recruitment to STING activates both IRF3 and NF- κ B that mediate immune defense against tumors and viral infections. *Proc Natl Acad Sci U S A* 118
- Zhang J, Hu MM, Wang YY & Shu HB (2012) TRIM32 protein modulates type I interferon induction and cellular antiviral response by targeting MITA/STING protein for K63-linked ubiquitination. *J Biol Chem* 287: 28646–55
- Zhong B, Yang Y, Li S, Wang Y-Y, Li Y, Diao F, Lei C, He X, Zhang L, Tien P, *et al* (2008) The Adaptor Protein MITA Links Virus-Sensing Receptors to IRF3 Transcription Factor Activation. *Immunity* 29: 538–550

Figure Legends

Figure 1. STING activation induces M1 and K63 ubiquitin chain formation.

- A)** Representative Airyscan-processed confocal images of Wild-type (WT) HeLa cells stably expressing BFP-P2A-STING (HeLa^{STING}) and mEGFP-LC3B (green) treated with 60 μ g/mL of cGAMP for 8 hours prior to PFA-fixation and immunostaining with antibodies raised against mono- and poly-ubiquitin chains (Ub; magenta) and STING (cyan). Scale bar = 10 μ m, and 2 μ m (inset). Imaging was replicated in >3 independent experiments.
- B)** Quantification of the percentage (%) of cells positive for mEGFP-LC3B foci and immunostained Ub foci (left panel), and the percentage (%) of mEGFP-LC3B foci with overlapping immunolabeled signal for Ub, STING, or both (right panel) from experiments represented in Fig. EV1A, and similar conditions to Fig. 1A. Error bars represent +/- s.d. from 3 replicates analyzed in the same experiment. Imaging was replicated in 3 independent experiments.
- C-F)** Representative immunoblots of indicated proteins detected in HeLa^{STING} cell lysates prepared after treatment with 120 μ g/mL cGAMP for 8 hours. Immunoblotting was replicated in 3 independent experiments.
- G)** Quantification of immunoblots in (D-F). Values represent relative intensity of cGAMP treated to untreated lanes. Error bars represent mean +/- s.d. of three independent experiments.
- H)** Quantification of ubiquitin-GG linked peptides from lysate (left) and Pan-TUBE (Tandem-Ubiquitin Binding Entities) enriched samples (right) identified by targeted LC-MS/MS. HeLa^{STING} cells stably expressing mEGFP-

LC3B were treated with 120 $\mu\text{g}/\text{mL}$ of cGAMP for 8 hours prior to cell lysis, Pan-TUBE enrichment, and LC-MS/MS analysis. Mass spectrometry data from cell lysates are from 2 independent experiments with 3-5 technical replicates each. Pan-TUBE enrichment was performed in technical triplicate from one of the same cell lysates analyzed in the left panel. Values represent relative amount of peptides detected in cGAMP treated cells over untreated cells. Error bars represent \pm s.d. from replicates described above.

I) Representative Airyscan-processed confocal images of HeLa^{STING}; mEGFP-LC3B (green) cells treated with 100 μM Monensin for 1 hour prior to PFA-fixation and immunostaining with antibodies raised against mono- and poly-ubiquitin chains (Ub; magenta). Scale bar = 10 μm , and 2 μm (inset). Imaging was replicated in 2 independent experiments.

J-K) Representative immunoblots for indicated linkage specific ubiquitin chains in HeLa^{STING} cell lysates prepared after treatment with 100 μM Monensin for 1 hour. Immunoblotting was replicated in 3 independent experiments.

L) Quantification of immunoblots in (J-K). Values represent relative intensity of Monensin treated to untreated lanes. Error bars represent mean \pm s.d. of three independent experiments.

Expanded View 1.

A) Representative spinning disk confocal images of HeLa^{STING}; mEGFP-LC3B (green) cells treated with 120 $\mu\text{g}/\text{mL}$ of cGAMP for 8 hours prior to PFA-fixation and immunostaining for mono- and poly-ubiquitin chains (Ub; magenta), and STING (cyan). Scale bar = 20 μm . Corresponding to quantification in Fig. 1B.

B) Representative spinning disk confocal images of HeLa^{STING}; mEGFP-LC3B (green) cells treated with 1 μM diABZI for 4 hours prior to PFA-fixation and immunostaining for mono- and poly-ubiquitin chains (Ub; magenta), and STING (cyan). Scale bar = 20 μm . Corresponding to quantification in Fig. EV1C.

C) Quantification of the percentage (%) of cells positive for mEGFP-LC3B foci and immunostained Ub foci (left panel), and the percentage (%) of mEGFP-LC3B foci with overlapping immunolabeled signal for Ub, STING, or both (right panel) from experiments represented in Fig. EV1B. Error bars represent \pm s.d. from 3 replicates analyzed in the same experiment. Imaging was replicated in 3 independent experiments.

D-E) Representative spinning disk confocal images of HeLa^{STING}; mEGFP-LC3B cells treated with 120 µg/mL of cGAMP for 8 hours prior to PFA-fixation and immunostaining for K48- and K63-ubiquitin chains. Scale bar = 20 µm.

F) Quantification of the percentage (%) of mEGFP-LC3B foci with overlapping signal for immunolabeled K48- and K63-ubiquitin chain from experiments represented in Fig. EV1D-E. Error bars represent +/- s.d. from 3 replicates analyzed in the same experiment. Imaging was replicated in 3 independent experiments.

G) Pearson's correlation coefficient of mScarlet1-LC3B and Vx3-EGFP over time in the live imaging experiment represented in Movie 1. FRT/TREX HeLa cells stably expressing FRT/TO-DD-Vx3-EGFP, BFP-P2A-STING, and mScarlet1-LC3B were incubated with 1 µg/mL Doxycycline and 500 nM Shield1 for 24 hours prior to treatment with either 120 µg/mL cGAMP or 1 µM diABZI and imaging every 30 minutes for 12 hours on a spinning disk confocal microscope. Error bars represent +/- s.d. from 3 replicates analyzed in the same experiment. Imaging was replicated in 3 independent experiments.

Figure 2. HOIP mediates STING activation induced M1 ubiquitin chain formation.

A) Representative Airyscan-processed confocal images of HeLa^{STING} cells stably expressing mScarlet1-LC3B (magenta) and mEGFP-HOIP (green) treated with 120 µg/mL of cGAMP for 8 hours prior to saponin extraction and PFA-fixation. Scale bar = 10 µm, and 2 µm (inset). Imaging was replicated in 3 independent experiments. Representative images from non-saponin extracted cells are in Fig. EV2A.

B) Quantification of the percentage (%) of mEGFP-LC3B foci with overlapping immunolabeled signal for HOIP, or HOIP and STING, from experiments represented in Fig. EV2B, and corresponding conditions to Fig. 2A. Error bars represent +/- s.d. from 3 replicates analyzed in the same experiment. Imaging was replicated in 3 independent experiments. Representative images are in Fig. EV2B.

C) Representative immunoblots of indicated proteins detected in HeLa^{STING} cell lysates from WT, HOIPKO, and HOIPKO stably expressing untagged HOIP prepared following treatment with 120 µg/mL cGAMP for 8 hours. Immunoblotting was replicated in 3 independent experiments.

D) Quantification of M1-Ub in (C). Values represent relative intensity of corresponding lanes to WT untreated lanes. Error bars represent mean +/- s.d. of three independent experiments.

E) Representative immunoblots of indicated proteins detected in THP1 cell lysates from WT, HOIPKO^{pool}, and HOIPKO^{pool} stably expressing untagged HOIP prepared following treatment with 1 μ M diABZI for 4 hours. Immunoblotting was replicated in 3 independent experiments.

F) Quantification of M1-Ub in (E). Values represent relative intensity of corresponding lanes to WT untreated lanes. Error bars represent mean \pm s.d. of three independent experiments.

G) Representative immunoblots of indicated proteins detected in THP1 cell lysates from WT and HOIPKO^{pool} cells prepared following treatment with 1 μ M diABZI for 1, 2, 4, and 8 hours. Immunoblotting was replicated in 3 independent experiments.

H) Representative immunoblots of indicated proteins detected in iBMDM cell lysates from shCtrl and shHOIP cells prepared following treatment with 0.2 μ M diABZI for 1, 2, and 4 hours. Immunoblotting was replicated in 3 independent experiments.

I) Quantification of M1-Ub in (H). Values represent relative intensity of corresponding lanes to untreated lanes per cell line. Error bars represent mean \pm s.d. of three independent experiments.

Expanded View 2.

A) Representative Airyscan-processed confocal images of HeLa^{STING} cells stably expressing mScarlet1-LC3B and mEGFP-HOIP treated with 120 μ g/mL of cGAMP for 8 hours with no saponin extraction prior to PFA-fixation. Scale bar = 10 μ m. Corresponding to representative images in Fig. 2A. Imaging was replicated in 3 independent experiments.

B) Representative spinning disk confocal images of HeLa^{STING}; mEGFP-HOIP (green); mScarlet1-LC3B (magenta) cells treated with 120 μ g/mL of cGAMP for 8 hours prior to saponin extraction and PFA-fixation. Scale bar = 20 μ m. Corresponding to quantification in Fig. 2B.

C-D) Representative immunoblots of indicated proteins detected in cell lysates from HeLa^{STING} WT and HOIPKO cells (C) or HeLa^{STING} and HeLa^{STING} stably expressing mEGFP-OTULIN (D) prepared following treatment with 120 μ g/mL cGAMP for 8 hours. Immunoblotting was replicated in 3 independent experiments.

E-F) Representative immunoblots of indicated proteins detected in HeLa^{STING} cell lysates from WT and HOIPKO cells prepared following treatment with 120 μ g/mL cGAMP (E) or 1 μ M diABZI (F) for 1, 2, 4, and 8 hours. Immunoblotting was replicated in 3 independent experiments.

G) Representative immunoblots of endogenous STING detected in cell lysates from WT and HOIPKO HeLa cells without stable overexpression of STING. Cells were treated with 15 $\mu\text{g}/\text{mL}$ cGAMP for 8 hours. Immunoblotting was replicated in 3 independent experiments.

H) Representative immunoblots of indicated proteins detected in THP1 cell lysates from WT and HOIPKO^{pool} cells prepared following treatment with 120 $\mu\text{g}/\text{mL}$ cGAMP for 1, 2, 4, and 8 hours. Immunoblotting was replicated in 3 independent experiments.

Figure 3. Loss of STING-mediated VAIL disrupts the perinuclear localization of ubiquitin and HOIP, but not M1-Ub chain formation.

A) Representative immunoblots of indicated proteins detected lysates from HeLa^{STING} WT and HeLa^{STING} with stable overexpression of mEGFP-SopF prepared after treatment with 120 $\mu\text{g}/\text{mL}$ cGAMP for 8 hours. Immunoblotting was replicated in 3 independent experiments.

B) Quantification of M1-Ub in (A). Values represent relative intensity of lanes to WT cGAMP-treated lanes. Error bars represent mean \pm s.d. of three independent experiments.

C) Representative Airyscan-processed confocal images of WT HeLa^{STING} cells stably expressing mScarletI-LC3B alone or with stable expression of mEGFP-SopF treated with 120 $\mu\text{g}/\text{mL}$ of cGAMP for 8 hours prior to PFA-fixation and immunostaining with antibodies raised against mono- and poly-ubiquitin chains (Ub). Scale bar = 20 μm . Imaging was replicated in 3 independent experiments.

D) Representative immunoblots of indicated proteins detected lysates from HeLa^{STING} WT and ATG16L1KO cells prepared after treatment with 120 $\mu\text{g}/\text{mL}$ cGAMP for 8 hours. Immunoblotting was replicated in 3 independent experiments.

E) Quantification of M1-Ub in (D). Values represent relative intensity of lanes to WT cGAMP-treated lanes. Error bars represent mean \pm s.d. of three independent experiments.

F) Representative spinning disk confocal images of HeLa^{STING}; mEGFP-HOIP (green); mScarletI-LC3B (orange) cells treated with 120 $\mu\text{g}/\text{mL}$ of cGAMP for 8 hours prior to prior to saponin extraction, PFA-fixation and immunostaining for ubiquitin (Ub; magenta). Scale bar = 20 μm .

G) Quantification and distribution of the number and size of HOIP (top) and Ubiquitin punctae (bottom) in the experiment represented in (F). Large ‘punctae’ can be interpreted as ‘foci’. Imaging was replicated in 3 independent experiments.

Expanded View 3.

A) Representative Airyscan-processed confocal images of HeLa^{STING} and HeLa^{STING} cells with stable overexpression of mEGFP-LC3B (green) treated with 120 µg/mL of cGAMP for 8 hours prior to PFA-fixation and immunostaining with antibodies raised against mono- and poly-ubiquitin chains (Ub; magenta) and STING (cyan). Scale bar = 20 µm, and 2 µm (inset). Imaging was replicated in 2 independent experiments.

B) Representative immunoblots of indicated proteins detected lysates from HeLa^{STING} WT and HeLa^{STING} with stable overexpression of mEGFP-LC3B prepared after treatment with 120 µg/mL cGAMP for 8 hours. Immunoblotting was replicated in 3 independent experiments.

C) Representative immunoblots of indicated proteins detected in HeLa^{STING} cell lysates prepared after treatment with either DMSO, 10 µM C53, 1 µM diABZI, or both C53 and diABZI for 4 hours. Immunoblotting was replicated in 3 independent experiments.

D-E) Representative spinning disk confocal images of FRT/TREX HeLa cells stably expressing FRT/TO-DD-Vx3-EGFP, BFP-P2A-STING, and mScarlet-LC3B at the 6-hour timepoint following treatment (D) and quantification of the percentage (%) of cells positive for Vx3-EGFP foci over time (E). Cells were incubated with 1 µg/mL Doxycycline and 500 nM Shield1 for 24 hours prior to treatment with either DMSO, 10 µM C53, 1 µM diABZI, or both C53 and diABZI, and imaging every 30 minutes for 12 hours on a spinning disk confocal microscope. Scale bar = 50 µm. Quantification is from 3 wells analyzed in the same experiment. Imaging was replicated in 2 independent experiments.

Figure 4. M1 ubiquitin chains stimulate STING-mediated NFκB-related immune signaling.

A) Representative immunoblots of indicated proteins detected in THP1 cell lysates from WT and HOIPKO^{pool} cells prepared following treatment with 1 µM diABZI for 1, 2, 4, and 8 hours. Immunoblotting was replicated in 3 independent experiments.

B) Quantification of pI κ B α ^{S32} in (A). Values represent relative intensity of corresponding bands to untreated bands per cell line. Replicates for each condition from 2 independent experiments are shown.

C) Quantification of pI κ B α ^{S32} in (D). Values represent relative intensity of bands to WT treated bands. Error bars represent mean +/- s.d. of three independent experiments.

D) Representative immunoblots of indicated proteins detected in THP1 cell lysates from WT, HOIPKO^{pool}, and HOIPKO^{pool} stably expressing untagged HOIP prepared following treatment with 1 μ M diABZI for 4 hours. Immunoblotting was replicated in 3 independent experiments.

E-F) Relative expression changes of indicated NF κ B- (E) and IRF3/interferon-related (F) genes detected by quantitative RT-PCR in WT and HOIPKO^{pool} THP1 cells treated with 1 μ M diABZI for 1, 2, 4, and 8 hours. Quantification of relative expression is from 3 independent experiments analyzed at the same time. A 2-way ANOVA with a Tukey's multiple comparisons test was performed on $2^{-\Delta\Delta Ct}$ values. Error bars represent s.d. * <0.05 , ** <0.01 , *** <0.001 , **** <0.0001 .

G-H) Relative expression changes of indicated NF κ B- (G) and IRF3/interferon-related (H) genes detected by quantitative RT-PCR in THP1 WT, HOIPKO^{pool}, and HOIPKO^{pool} stably expressing untagged HOIP cells treated with 1 μ M diABZI for 4 hours. Quantification of relative expression is from 4 independent experiments analyzed at the same time. A 2-way ANOVA with a Tukey's multiple comparisons test was performed on $2^{-\Delta\Delta Ct}$ values. Error bars represent s.d. * <0.05 , ** <0.01 , *** <0.001 , **** <0.0001 .

Expanded View 4.

A) Representative immunoblots of indicated proteins detected in THP1 cell lysates from WT and HOIPKO^{pool} cells prepared following treatment with 120 μ g/mL cGAMP for 1, 2, 4, and 8 hours. Immunoblotting was replicated in 3 independent experiments.

B-C) Relative expression changes of indicated NF κ B- (B) and IRF3/interferon-related (C) genes detected by quantitative RT-PCR in WT and HOIPKO^{pool} THP1 cells treated with 120 μ g/mL cGAMP for 1, 2, 4, and 8 hours. Quantification of relative expression is from 3 independent experiments analyzed at the same time. A 2-way ANOVA with a Tukey's multiple comparisons test was performed on $2^{-\Delta\Delta Ct}$ values. Error bars represent s.d. * <0.05 , ** <0.01 , *** <0.001 , **** <0.0001 .

D-E) Relative expression changes of indicated NF κ B- (D) and IRF3/interferon-related (E) genes detected by quantitative RT-PCR in WT and shCtrl and shHOIP iBMDM cells treated with 0.2 μ M diABZI for 1, 2, and 4 hours. Quantification of relative expression is from 3 independent experiments analyzed at the same time. A 2-way ANOVA with a Tukey's multiple comparisons test was performed on $2^{-\Delta\Delta C_t}$ values. Error bars represent s.d. * <0.05 , ** <0.01 , *** <0.001 , **** <0.0001 .

Figure 5. LC3B lipidation is not required for STING-mediated innate immune responses.

A) Representative immunoblots of indicated proteins detected in THP1 cell lysates from WT and ATG16L1KO cells prepared following treatment with 1 μ M diABZI for 1, 2, and 4 hours. Immunoblotting was replicated in 3 independent experiments.

B-C) Relative expression changes of indicated NF κ B- (B) and IRF3/interferon-related (C) genes detected by quantitative RT-PCR in WT and ATG16L1KO THP1 cells treated with 1 μ M diABZI for 2, 4, 6, and 8 hours. Quantification of relative expression is from 3 independent experiments analyzed at the same time. A 2-way ANOVA with a Tukey's multiple comparisons test was performed on $2^{-\Delta\Delta C_t}$ values. Error bars represent s.d. * <0.05 , ** <0.01 , *** <0.001 , **** <0.0001 .

Expanded View 5.

A) Representative immunoblots of indicated proteins detected in THP1 cell lysates from WT and ATG16L1KO cells prepared following treatment with 1 μ M diABZI for 1, 2, and 4 hours. Immunoblotting was replicated in 3 independent experiments.

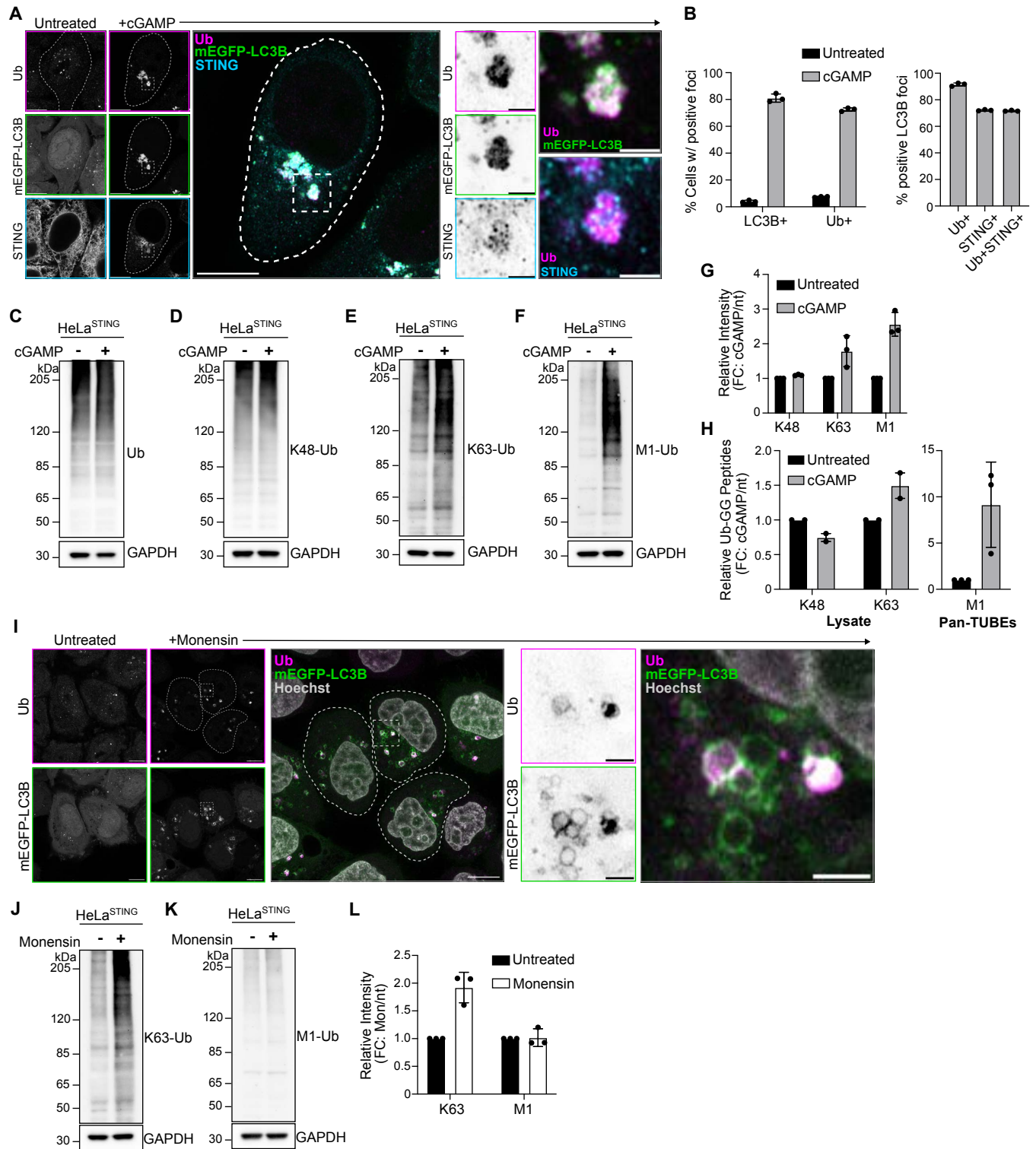
B) Representative immunoblots of indicated proteins detected in lysates from WT THP1 cells prepared following treatment with either DMSO, 10 μ M C53, 1 μ M diABZI, or both C53 and diABZI for 4 hours. Immunoblotting was replicated in 3 independent experiments.

C-D) Relative expression changes of indicated NF κ B-related genes (C) and interferon-related genes (D) detected by quantitative RT-PCR in THP1 cells treated with DMSO, 10 μ M C53, 1 μ M diABZI, or both C53 and diABZI for 4 hours. Quantification of relative expression is from 4 independent experiments analyzed at the same time. A one-way ANOVA with a Tukey's multiple comparisons test was performed on $2^{-\Delta\Delta C_t}$ values. Error bars represent Standard Deviation. * <0.05 , ** <0.01 , *** <0.001 , **** <0.0001 .

Movie 1.

Representative spinning disk confocal movie of FRT/TREX HeLa cells stably expressing FRT/TO-DD-Vx3-EGFP, BFP-P2A-STING, and mScarlet-LC3B. Cells were incubated with 1 $\mu\text{g}/\text{mL}$ Doxycycline and 500 nM Shield1 for 24h prior to treatment with 120 $\mu\text{g}/\text{mL}$ cGAMP and imaging every 30 minutes for 12 hours on a spinning disk confocal microscope. Scale bar = 25 μm .

Figure 1



Expanded Figure 1

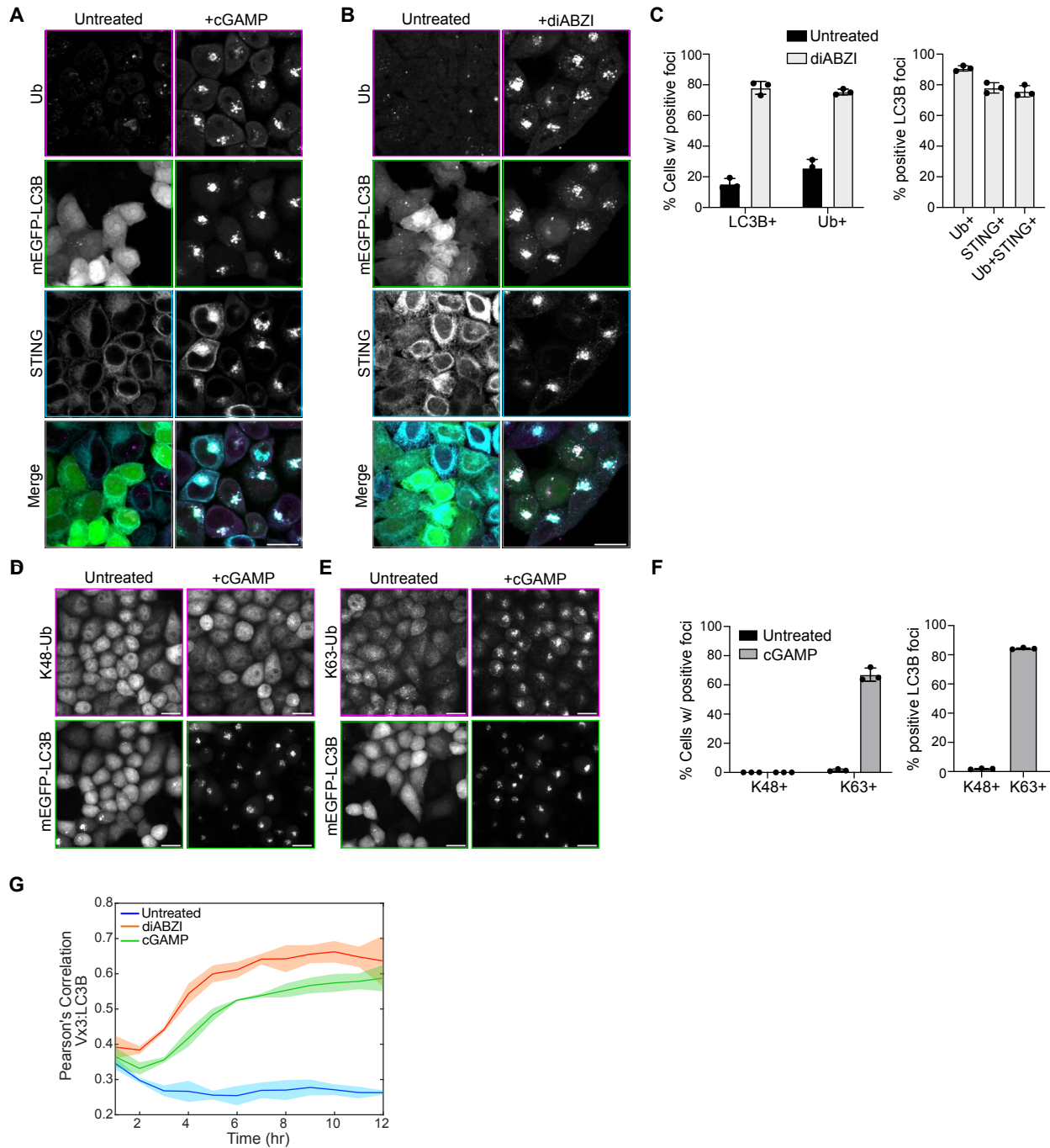


Figure 2

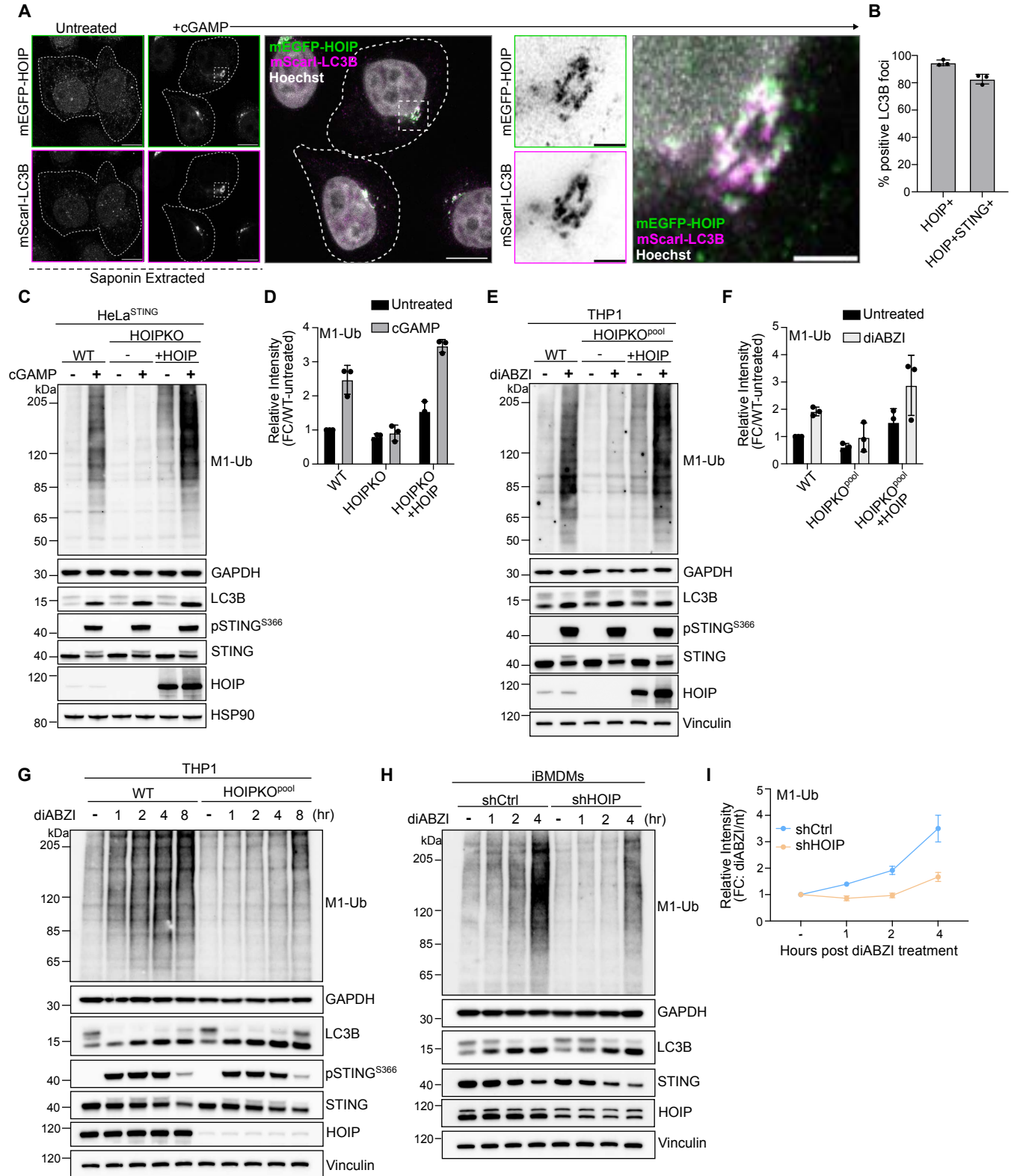
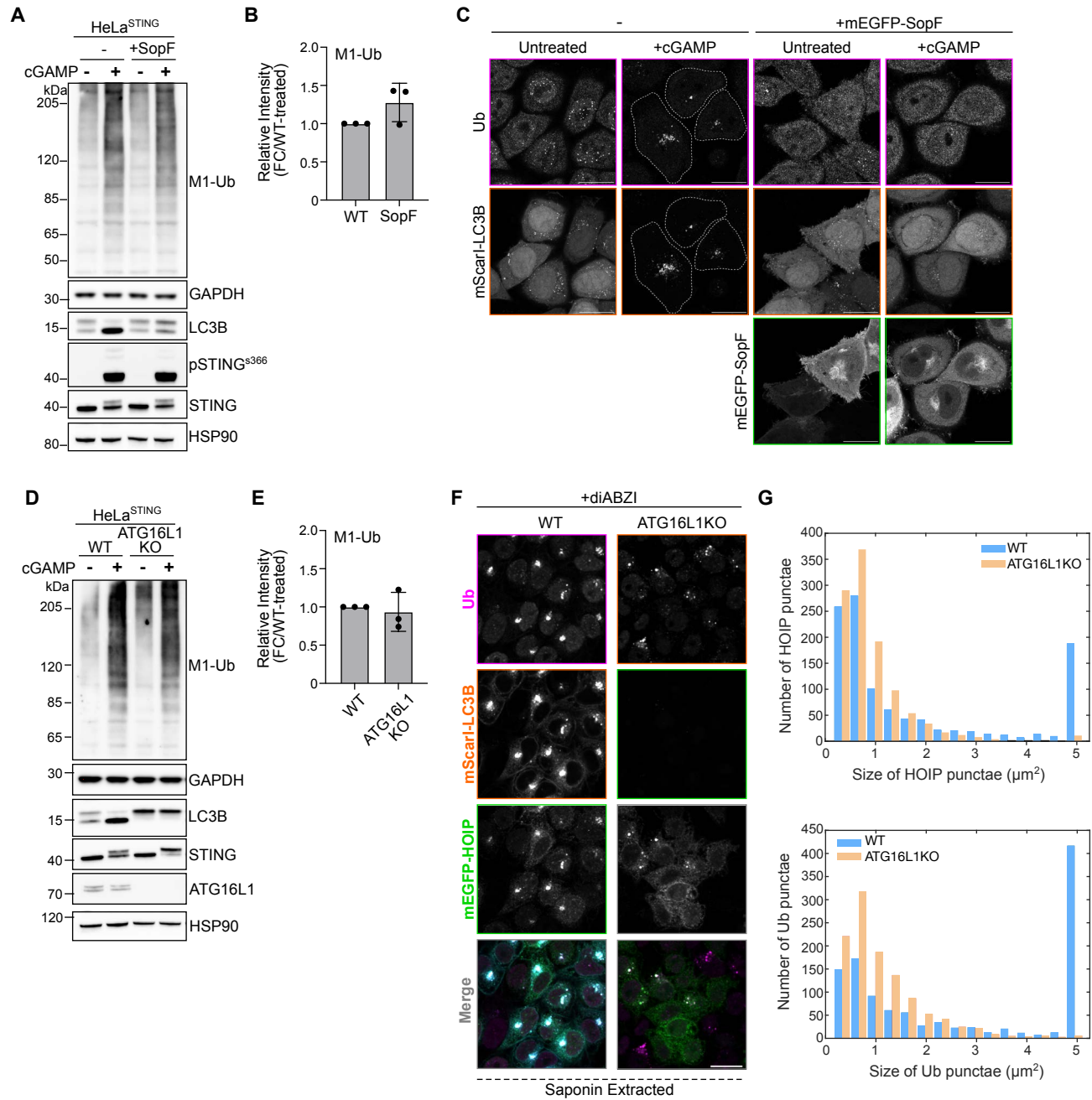


Figure 3



Expanded Figure 3

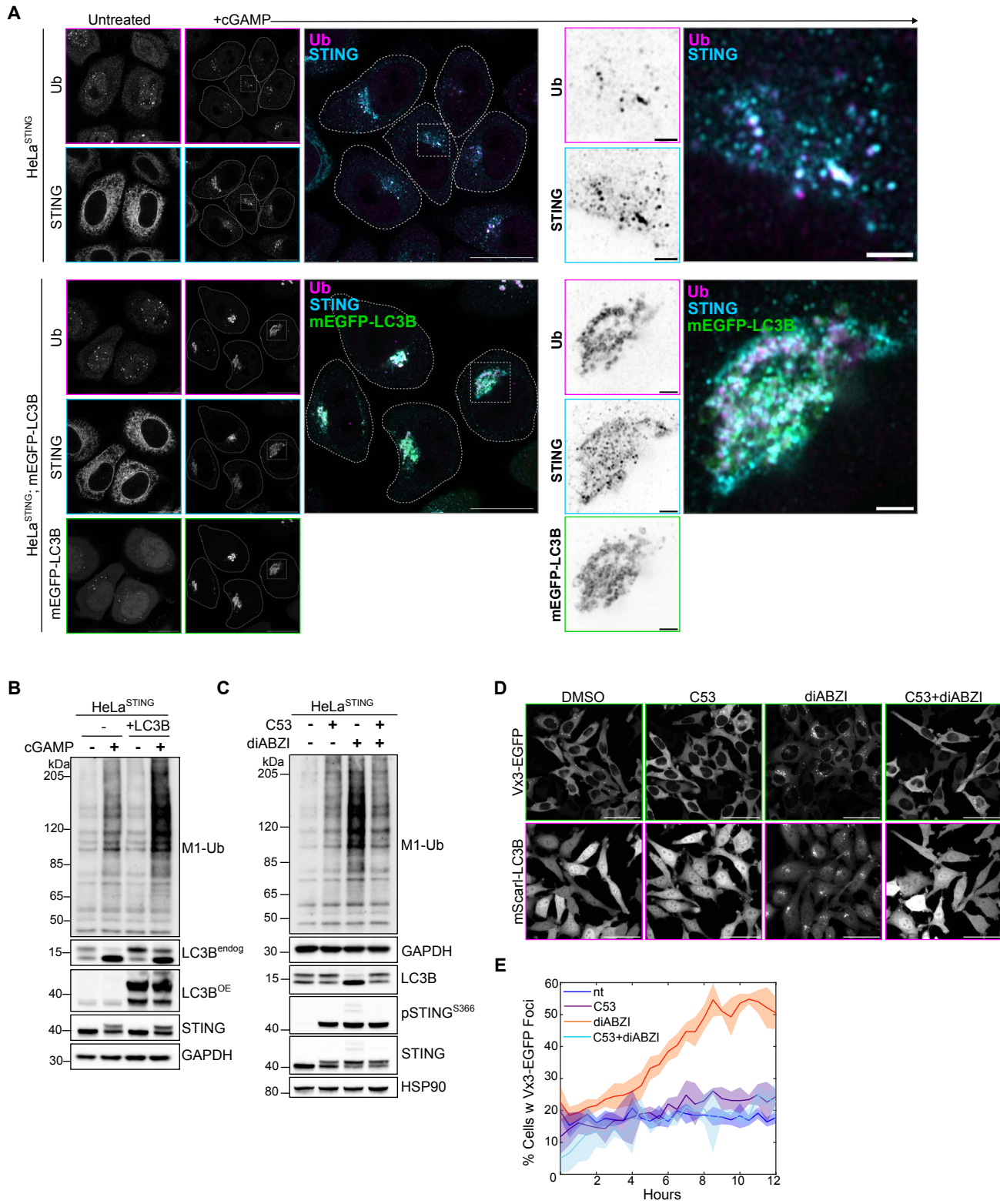
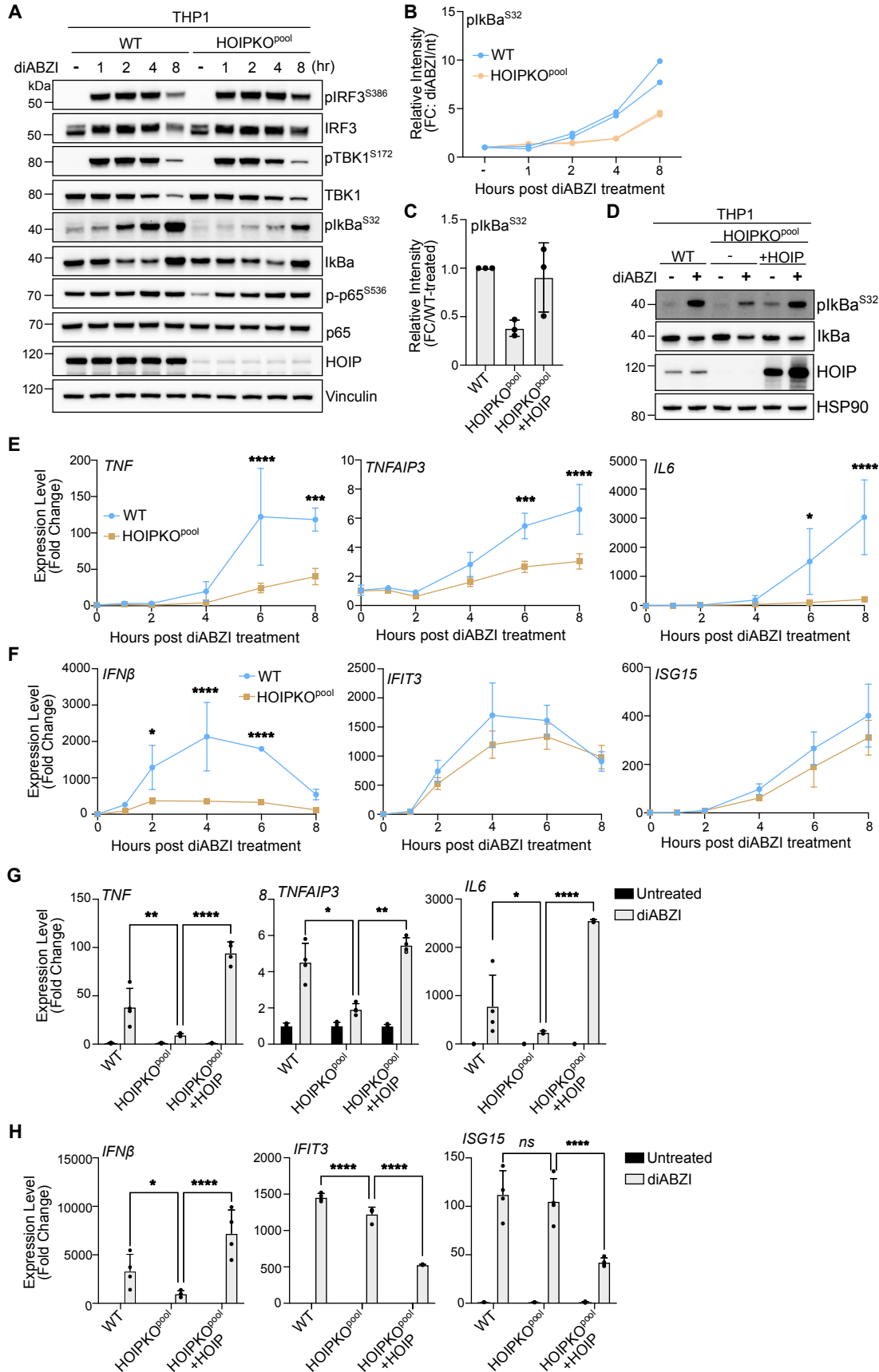
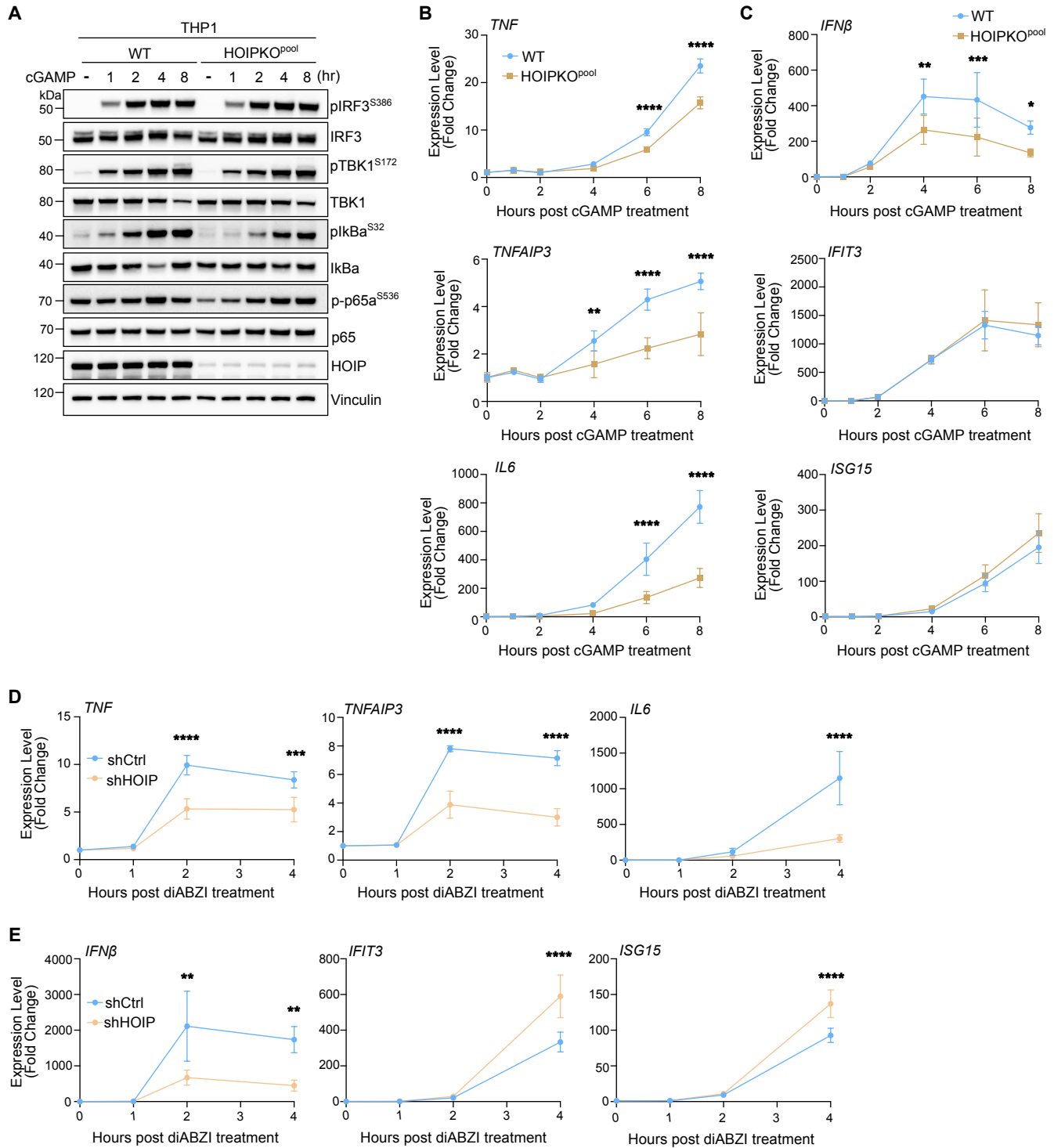


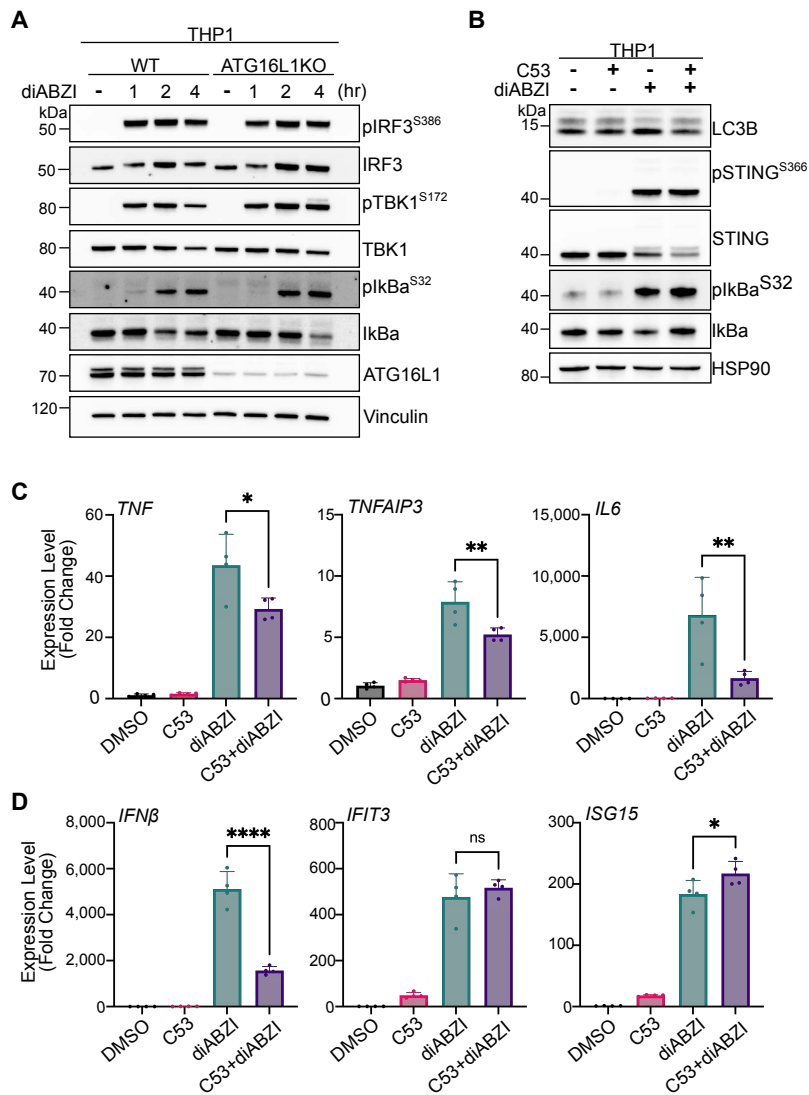
Figure 4



Expanded Figure 4



Expanded Figure 5



Appendix

Table of Contents:

Figure S1.

Figure S2.

Appendix Figure S1.

A-B) Representative immunoblots of indicated proteins detected in WT and HOIPKO HeLa cell lysates prepared following treatment with 120 $\mu\text{g}/\text{mL}$ cGAMP (A) or 1 μM diABZI (B) for 1, 2, 4, and 8 hours.

Immunoblotting was replicated in 3 independent experiments.

C) Representative immunoblots of indicated proteins detected in lysates from HeLa^{STING} and HeLa^{STING} cells with stable overexpression of mEGFP-OTULIN prepared following treatment with 120 $\mu\text{g}/\text{mL}$ cGAMP for 8 hours. Immunoblotting was replicated in 3 independent experiments.

D-E) Relative expression of indicated NF κ B-related genes (D) and IRF3/interferon-related genes (E) detected by quantitative RT-PCR in HeLa^{STING}: WT, HOIPKO, and HOIPKO stably expressing mEGFP-HOIP cells treated with 120 $\mu\text{g}/\text{mL}$ cGAMP for 8 hours. Quantification of relative expression is from 3 independent experiments analyzed at the same time. A 2-way ANOVA with a Tukey's multiple comparisons test was performed on $2^{-\Delta\Delta\text{Ct}}$ values. Error bars represent Standard Deviation. * <0.05 , ** <0.01 , *** <0.001 , **** <0.0001 **F)**

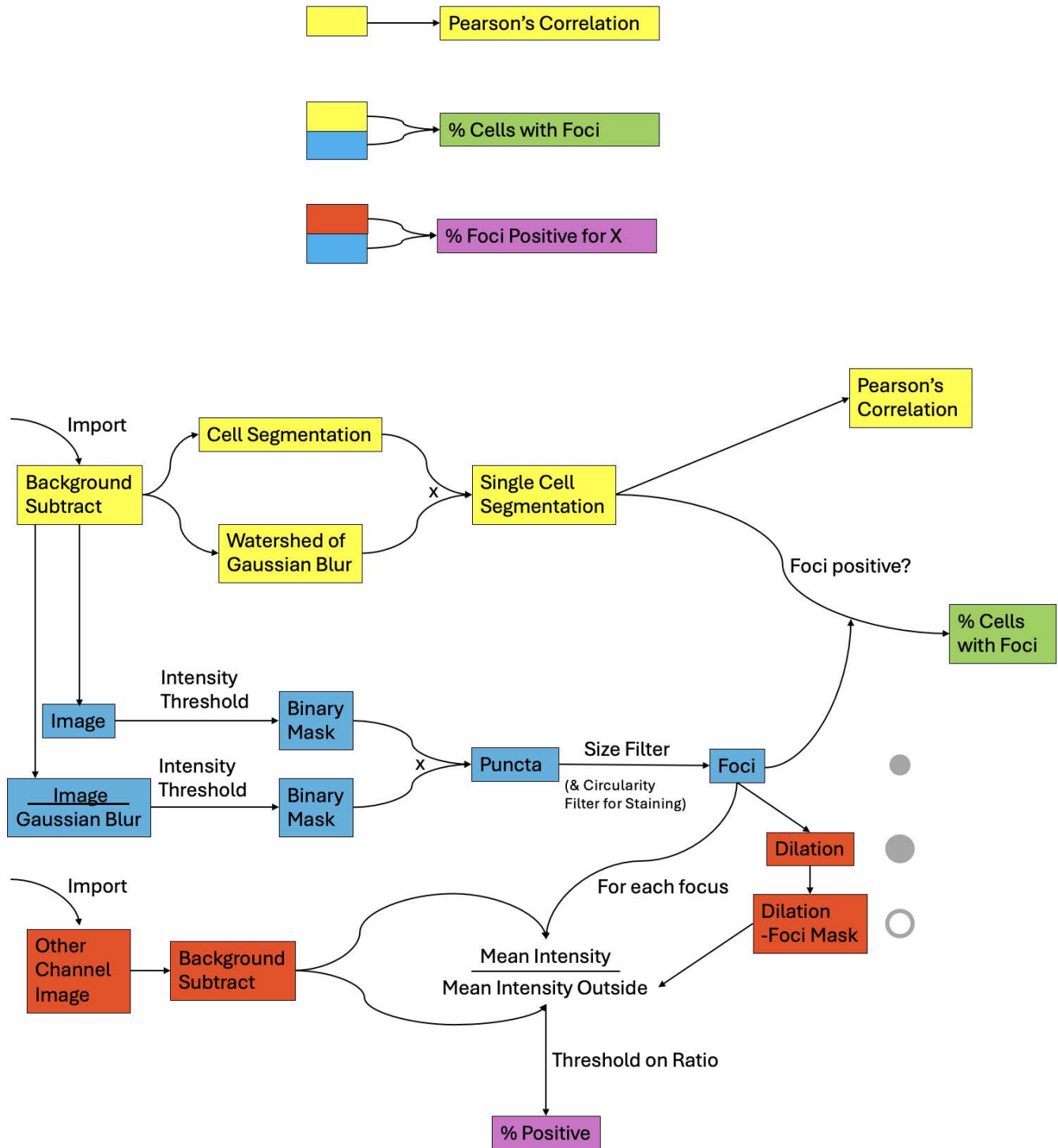
Relative expression of indicated NF κ B-related genes detected by quantitative RT-PCR in HeLa^{STING} WT, HOIPKO, and HOIPKO stably expressing mEGFP-HOIP cells treated with 10 ng/mL TNF α for 30 minutes. Quantification of relative expression is from 3 independent experiments analyzed at the same time. A 2-way ANOVA with a Tukey's multiple comparisons test was performed on $2^{-\Delta\Delta\text{Ct}}$ values. Error bars represent Standard Deviation. * <0.05 , ** <0.01 , *** <0.001 , **** <0.0001 .

F) Relative expression of indicated NF κ B-related genes detected by quantitative RT-PCR in HeLa^{STING}: WT, HOIPKO, and HOIPKO stably expressing mEGFP-HOIP cells treated with 10 ng/mL TNF α for 30 minutes. Quantification of relative expression is from 3 independent experiments analyzed at the same time. A 2-way ANOVA with a Tukey's multiple comparisons test was performed on $2^{-\Delta\Delta\text{Ct}}$ values. Error bars represent Standard Deviation. * <0.05 , ** <0.01 , *** <0.001 , **** <0.0001 .

G-H) Relative expression of indicated NF κ B-related genes (G) and interferon-related genes (H) detected by quantitative RT-PCR in WT HeLa^{STING} and WT HeLa^{STING} cells stably overexpressing mEGFP-OTULIN treated with 120 $\mu\text{g}/\text{mL}$ cGAMP for 8 hours. Quantification of relative expression is from 3 independent experiments analyzed at the same time. A 2-way ANOVA with a Tukey's multiple comparisons test was performed on $2^{-\Delta\Delta\text{Ct}}$ values. Error bars represent Standard Deviation. * <0.05 , ** <0.01 , *** <0.001 , **** <0.0001 .

I) Relative expression of indicated NF κ B-related genes detected by quantitative RT-PCR in HeLa^{STING} and HeLa^{STING} cells with stable overexpression of mEGFP-OTULIN treated with 10 ng/mL TNF α for 30 minutes. Quantification of relative expression is from 3 independent experiments analyzed at the same time. A 2-way ANOVA with a Tukey's multiple comparisons test was performed on $2^{-\Delta\Delta C_t}$ values. Error bars represent Standard Deviation. * <0.05 , ** <0.01 , *** <0.001 , **** <0.0001 .

Appendix Figure S2



Appendix Figure S2.

Schematic of MATLAB workflow for image analysis.